Published for SISSA by Springer

Received: *June 3, 2011*
Accepted: *October 5, 2011*
Published: *October 14, 2011*

Towards $pp \to VVjj$ at NLO QCD: bosonic contributions to triple vector boson production plus jet

Francisco Campanario

Institut für Theoretische Physik, Universität Karlsruhe, KIT, 76128 Karlsruhe, Germany

E-mail: francam@particle.uni-karlsruhe.de

Abstract: In this work, some of the NLO QCD corrections for $pp \to VVjj + X$ are presented. A program in Mathematica based on the structure of FeynCalc which automatically simplifies a set of amplitudes up to the hexagon level of rank 5 has been created for this purpose. We focus on two different topologies. The first involves all the virtual contributions needed for quadruple electroweak vector boson production, i.e. $pp \to VVVV + X$. In the second, the remaining "bosonic" corrections to electroweak triple vector boson production with an additional jet ($pp \to VVVj + X$) are computed. We show the factorization formula of the infrared divergences of the bosonic contributions for VVVV and VVVj production with $V \in (W, Z, \gamma)$. Stability issues associated with the evaluation of the hexagons up to rank 5 are studied. The CPU time of the FORTRAN subroutines rounds the 2 milliseconds and seems to be competitive with other more sophisticated methods. Additionally, in appendix A the master equations to obtain the tensor coefficients up to the hexagon level in the external momenta convention are presented including the ones needed for small Gram determinants.

Keywords: NLO Computations, QCD

ArXiv ePrint: 1105.0920

doi:10.1007/JHEP10(2011)070

JHEP10(2011)070

Contents

JHEP10(2011)070

1 Introduction

The incoming data from the CERN Large Hadron Collider (LHC) will require precise theoretical predictions for a variety of signal and background processes. Processes with two vector bosons are of vital importance since they constitute background signals to Higgs and top physics as well as to physics Beyond the Standard Model (BSM) (for an overview see e.g. ref. [1]). A tremendous effort has been carried out by the scientific community to compute these processes accurately. Next-to-Leading Order (NLO) QCD diboson production was computed in refs. [2–9], and with an additional jet in refs. [10–16]. Diboson production in association with two jets can occur through both electroweak (EW) and QCD mechanism. The NLO QCD corrections for EW production, including the leptonic decays of the weak bosons, $\mathcal{O}(\alpha_s\alpha^6)$, was computed in refs. [17–19] considering only the dominant t-channel production contributions. Recently, the NLO QCD corrections to $W^+W^+jj + X$ [20] and $W^+W^-jj + X$ [21] production through the pure QCD mechanism including the leptonic decays of the weak boson, $\mathcal{O}$ $(\alpha_s^3\alpha^4)$, were computed using the generalized D-dimensional unitarity framework for the calculation of the one loop virtual amplitudes. The interference effects between the EW and QCD production mechanism have been estimated to be negliglible [21] and have not been computed. Also, results at NLO QCD for $W^+W^-b\bar{b}+X$ via QCD production have been presented using a spin-correlated narrow width approximation for the leptonic decays of the W-bosons in ref. [22] and without this approximation in ref. [23].

Figure 1. "One loop fermion" contributions (left) and "bosonic" contributions (right).

An impressive progress in the calculation of multi-parton one-loop amplitudes has been achieved not only applying new techniques [24–54], but also based on traditional methods [55–81]. In this paper, relying on traditional techniques, we compute some of the virtual corrections needed for $pp \to VVjj + X$ production. We focus on some of the topologies that appear, namely QCD "bosonic" one-loop corrections to the diagrams contributing to $pp \to VVVV + X$ and $pp \to VVVj + X$ production. The strategy followed is to collect Feynman diagrams with a given topology in groups which can be easily checked and reused in other processes. Thus, our aim is not only to provide results for $VVjj + X$ production, including a second calculation of $W^+W^-jj + X$ production through the pure QCD mechanism using a different method, but also to provide a set of routines that can be used for many other interesting processes, such as $W\gamma\gamma j + X$ at NLO QCD [82]. It is known that in the calculation of one-loop multi-leg amplitudes, the presence of small Gram and Cayley determinants might yield unstable results. In this paper, we show that the use of higher precision in the numerical determination of the tensor integrals (similarly to ref. [83]) together with the use of Ward Identities to identify the unstable points, and to a minor extent, following ref. [70], the use of special routines for the determination of small Gram determinants for the C and D functions, solve this problem.

The paper is organized as follows; in section 2, the method used to perform the calculation, the different contributions computed and the tests performed to guarantee the correctness of the results are described. In section 3, a discussion of the instabilities and the timing of the amplitudes computed are shown. The conclusions are given in section 4. In appendix A, the tensor reduction routines used are presented. In appendix B, numbers for the contributions involving the hexagons are given, including proofs of the factorization of the divergences and other additional numerical tests. Finally, in appendix C, we give the color factors needed for testing the amplitudes.

2 Calculational details

In the calculation of the NLO QCD virtual corrections to $pp \to VVjj + X$, different sub-processes contribute; processes involving two quark pairs, e.g., $uu \to ddW^+W^+$ and processes with one quark pair, e.g., $u\bar{u} \to W^+W^-gg$.[1] The latter can be separated into "one loop fermion" corrections and "bosonic" corrections, figure 1. Among the "bosonic"

[1]Note that the NLO QCD corrections for $pp \to W^+W^+jj + X$ production involve only sub-processes with two quark pairs.

JHEP10(2011)070

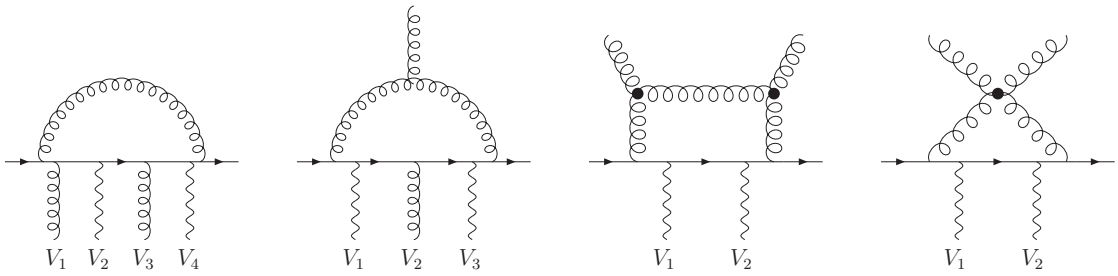

Figure 2. Different "bosonic" topologies. V_i stands for vector bosons emitted from the quark line.

contributions, different topologies appear, figure 2. We will focus on diagrams with the first two topologies, i.e., one loop QED-like corrections and diagrams formed with one triple gluon vertex. The remaining ones will be discussed in future publications.

To compute these amplitudes, a function in Mathematica [84] using FeynCalc [85] which automatically simplifies a set of amplitudes up to Hexagons of rank 5 has been created. Throughout the calculation, the quarks are considered to be massless, the anticommuting prescription for γ_5 is used and we work in the Feynman Gauge. The result is given in terms of tensor integrals following the Passarino-Veltman convention [55], appendix A, and written automatically in to FORTRAN routines. Nevertheless, the amplitudes can be evaluated also in Mathematica with unlimited precision which is used for testing purposes. To achieve that, the scalar integrals, the tensor reduction formalism to extract the tensor coefficient integrals, and also the helicity method described in refs. [86, 87] to compute the spinor products describing the quark lines of figure 2 have been implemented at the FORTRAN and Mathematica level. For the determination of the tensor integrals up to the box level, we have implemented the Passarino-Veltman tensor reduction formalism [55]. We have also applied the LU decomposition method to avoid the explicit calculation of inverse Gram matrices by solving a system of linear equations which is a more stable procedure close to singular points. Finally, for singular Gram determinants, special tensor reduction routines following ref. [70] have been implemented, however, the external momenta convention (Passarino-like) was used. The impact of these methods is discussed in detail in section 3. For pentagons, in addition to the Passarino-Veltman formalism, the method proposed by Denner and Dittmaier [70], applied also to hexagons, has been implemented. For that, the recursion relations of ref. [70] in terms of the Passarino-Veltman external momenta convention have been re-derived. This last method is used for the numerical implementation at the FORTRAN level in section 3. All the recursion relations used can be found in appendix A.

In the following, a more detailed description of the method used is given. To extract the rational terms, two simplifications are done at the Mathematica level. To illustrate them, the amplitude of a simple vertex diagram is used,

$$\mathrm{I} = \quad \overset{p_1}{\rightarrow} \quad l \quad \overset{p_3}{\leftarrow} \quad \uparrow p_2 \quad \mu_2 \qquad \propto \int \frac{d^d\, l}{(2\pi)^d} \frac{1}{l^2}\, \bar{v}(p_3)\gamma^\alpha \frac{(\not{l}+\not{p}_1+\not{p}_2)}{(l+p_1+p_2)^2}\gamma^{\mu_2} \frac{(\not{l}+\not{p}_1)}{(l+p_1)^2}\gamma_\alpha u(p_1).$$

JHEP10(2011)070

First, a simple Dirac re-ordering manipulation is applied to explicitly contract repeated indices and to obtain all the terms proportional to the space dimension, D, coming from $\gamma_\mu\gamma^\mu = D$ contractions, i.e.,

$$
\begin{aligned}
I &\propto \int \frac{d^d\, l}{(2\pi)^d} \frac{\bar{v}(p_3)\gamma^\alpha(\not{l}+\not{p}_1+\not{p}_2)\gamma^{\mu_2}(\not{l}+\not{p}_1)\gamma_\alpha u(p_1)}{(l+p_1+p_2)^2(l+p_1)^2 l^2} \\
&= \underbrace{-\int \frac{d^d\, l}{(2\pi)^d} \frac{\bar{v}(p_3)(\not{l})\gamma^{\mu_2}(\not{l})\overbrace{\gamma^\alpha\gamma_\alpha}^{D} u(p_1)}{(l+p_1+p_2)^2(l+p_1)^2 l^2}}_{II} + \ \ldots
\end{aligned}
\tag{2.1}
$$

Second, all Dirac's structure containing the loop momenta is pulled to the right, such that resulting terms like $\not{l}\not{l} = l^2$ are canceled against one of the integral denominators,

$$
\begin{aligned}
II \ &= \ D\, \bar{v}(p_3)\gamma^{\mu_2}u(p_1) \int \frac{d^d\, l}{(2\pi)^d} \frac{l^2}{l^2(l+p_1)^2(l+p_1+p_2)^2} + \ldots \\
&\propto \ D\, \bar{v}(p_3)\gamma^{\mu_2}u(p_1) I_2(p_2) + \ldots ,
\end{aligned}
\tag{2.2}
$$

where $I_2(p_2) \equiv B_0(p_2)$ is the scalar two point function defined correspondingly to eq. (A.1). In this way we avoid possible additional terms proportional to D coming from the Lorentz structure of the tensor integral. More concretely, the same term II could result in terms proportional to D^2:

$$
\begin{aligned}
II \ &= \ -D\, \bar{v}(p_3)\gamma_{\nu_1}\gamma^{\mu_2}\gamma_{\nu_2}u(p_1) \int \frac{d^d\, l}{(2\pi)^d} \frac{l^{\nu_1} l^{\nu_2}}{l^2(l+p_1)^2(l+p_1+p_2)^2} \\
&\propto \ -D\, \bar{v}(p_3)\gamma_{\nu_1}\gamma^{\mu_2}\gamma_{\nu_2}u(p_1) \times I^{(3)}_{00}(p_1,p_2) g^{\nu_1\nu_2} + \ldots \\
&= \ -(2-D)\, D\, \bar{v}(p_2)\gamma^{\mu_2}u(p_1) I^{(3)}_{00}(p_1,p_2) + \ldots ,
\end{aligned}
\tag{2.3}
$$

with $I^3_{00}(p_1,p_2) \equiv C_{00}(p_1,p_2)$, a three point tensor coefficient integral of the tensor integral $I^{\mu_1\mu_2}_3(p_1,p_2)$, defined by eq. (A.6), and obtained recursively from eq. (A.7). Further simplifications are obtained using the Dirac equation of motion and rewriting the pair $(l\cdot p_i)$ as a difference of two propagators, e.g., $(l\cdot p_1) = (l+p_1)^2 - l^2$, which are canceled against the denominators. The remaining rational terms stem from ultraviolet divergent tensor coefficients, which are treated independently within the tensor reduction routines. As an example, the finite contribution of the ultraviolet divergent tensor coefficient C_{00}, for massless propagators, following eq. (A.7) is obtained by,

$$
\begin{aligned}
C^{(\mathrm{fin})}_{00} &= \frac{1}{2D-4}\left(B_0 + \sum_{n=1}^{2}(r_n - r_{n-1})I^3_n\right)\Big|_{\mathrm{fin}} \\
&= \frac{1}{4}\left(B^{(\mathrm{fin})}_0 + \sum_{n=1}^{2}(r_n - r_{n-1})I^{3,(\mathrm{fin})}_n\right) + \frac{B^{(UV)}_0}{4},
\end{aligned}
\tag{2.4}
$$

where we have taken $D = 4 - 2\,\epsilon$ and series expand in ϵ all the scalar and tensor coefficient integrals, e.g.,

$$
B_0 = B^{(\mathrm{fin})}_0 + \frac{1}{\epsilon}B^{(UV)}_0,
\tag{2.5}
$$

JHEP10(2011)070

with $B_0^{(UV)} = 1$. After these steps, the amplitudes, $\mathcal{M}_v$, in terms of scalar and tensor coefficient integrals can be written by,

$$\mathcal{M}_v = \mathcal{M}_v^{D=4} + (D-4)\mathcal{M}_v^{DR}, \tag{2.6}$$

where $\mathcal{M}_v^{D=4}$ is the amplitude that one would obtain performing the Dirac algebra manipulation in four dimensions, $D = 4$, and $\mathcal{M}_v^{DR}$ contains the rational terms and vanish in Dimensional Reduction (DR). To get this expansion, we have only rewritten the space dimension D as $D = \bar{d} + 4$ such that for example eq. (2.2) is given by,

$$D\,\bar{v}(p_3)\gamma^{\mu_2}u(p_1)B_0(p_2) = \underbrace{4\,\bar{v}(p_3)\gamma^{\mu_2}u(p_1)B_0(p_2)}_{\mathcal{M}_v^{D=4}} + \bar{d}\,\underbrace{\bar{v}(p_3)\gamma^{\mu_2}u(p_1)B_0(p_2)}_{\mathcal{M}_v^{DR}}. \tag{2.7}$$

Both $\mathcal{M}_v^{D=4}$ and $\mathcal{M}_v^{DR}$ are decomposed in terms of,

$$\mathcal{M}^{(D=4,DR)} = \sum_{i,j,\tau} \mathrm{SM}_{i,\tau}\ \mathrm{F1}_j, \tag{2.8}$$

where $\mathrm{SM}_{i,\tau}$ is a basis of Standard Matrix elements corresponding to spinor products describing the quark line of figure 2 which are computed following the helicity method [86, 87] with a defined helicity, τ. $\mathrm{F1}_j$ are complex functions which are further decomposed into dependent and independent loop integral parts,

$$\mathrm{F1}_j = \sum_{l,k} \mathrm{F}_l T_k\Big(\epsilon(p_n)\cdot p_m; \epsilon(p_i)\cdot\epsilon(p_r)\Big). \tag{2.9}$$

T_k is a monomial function at most for each polarization vector $\epsilon(p_x)$, that is, $\epsilon(p_x)^0$ or $\epsilon(p_x)^1$. The first possibility, $\epsilon(p_x)^0$, implies that the polarization vector appears in the set of Standard Matrix elements, $\mathrm{SM}_{i,\tau}$. F_l contains kinematic variables $(p_i \cdot p_j)$, the scalar integrals $(B_0 \equiv I_2, C_0 \equiv I_3, D_0 \equiv I_4)$,[2] and the tensor integral coefficients $(B_{ij}, C_{ij}, D_{ij}, E_{ij}, F_{ij})$. The latter obtained numerically from the scalar integral basis following the recursion relations of appendix A. To illustrate this notation, the following example is given,

$$\begin{aligned}
&\bar{v}(p_4)\not{p}_2 P_+ u(p_1)\, C_0(p_1,p_2)\,\epsilon(p_3)\cdot\epsilon(p_2) + \bar{v}(p_4)\not{\epsilon}(p_2)P_+u(p_1)\, C_0(p_1,p_2)\,\epsilon(p_3)\cdot p_2 \qquad (2.10)\\
&= \underbrace{\bar{v}(p_4)\not{p}_2 P_+ u(p_1)}_{SM_{1,+}}\overbrace{\underbrace{C_0(p_1,p_2)}_{F_1}\underbrace{\epsilon(p_3)\cdot\epsilon(p_2)}_{T_1}}^{F1_1} + \underbrace{\bar{v}(p_4)\not{\epsilon}(p_2)P_+u(p_1)}_{SM_{2,+}}\overbrace{\underbrace{C_0(p_1,p_2)}_{F_1}\underbrace{\epsilon(p_3)\cdot p_2}_{T_2}}^{F1_2}\\
&= SM_{1,+}F1_1 + SM_{2,+}F1_2.
\end{aligned}$$

P_+ is the positive helicity projector, $P_+ = \frac{1+\gamma_5}{2}$. We note here that this parametrization is convenient for example to evaluate the amplitude for different polarization vectors or for performing gauge tests since some of the functions will remain unchanged. Finally, the full

[2] Note that throughout the paper to name the different n-point function integrals, I_n, the alphabetically-ordered labeling frequently found in the literature is also used.

JHEP10(2011)070

result is obtained from $\mathcal{M}_v^{D=4}$ and $\mathcal{M}_v^{DR}$ using the finite and the coefficients of the $1/\epsilon^n$ poles of the scalar and tensor coefficient integrals (see e.g. eq. (2.5)). From $\mathcal{M}_v^{D=4}$, we get

$$\mathcal{M}_v^{D=4} = \widetilde{\mathcal{M}}_v + \frac{\mathcal{M}_v^1}{\epsilon} + \frac{\mathcal{M}_v^2}{\epsilon^2}, \tag{2.11}$$

where $\widetilde{\mathcal{M}}_v$ is the finite contribution obtained using the finite pieces of the scalar and tensor coefficient integrals including the finite contributions from rational terms arising in ultraviolet tensor coefficient integrals, eqs. (2.4) and (A.7). $\mathcal{M}_v^1$ and $\mathcal{M}_v^2$ are obtained from the $1/\epsilon$ and $1/\epsilon^2$ pole contributions, respectively. Similarly, from $(D-4)\mathcal{M}^{DR}$, one gets,

$$(D-4)\mathcal{M}_v^{DR} = \widetilde{\mathcal{N}}_v + \frac{\mathcal{N}_v^1}{\epsilon}, \tag{2.12}$$

where $\widetilde{\mathcal{N}}_v$ and $\mathcal{N}_v^1$ are obtained from the $1/\epsilon$ and $1/\epsilon^2$ poles, respectively. Indeed, $\mathcal{N}_v^1$ is analytically zero since rational terms in one-loop QCD amplitudes, omitting wave renormalization graphs (WRF) are of UV origin [88]. Eq. (2.12) will allow us to check this statement numerically. Additionally, up to the pentagon level, the divergent part is computed in Dimensional Regularization analytically in Mathematica. A library containing all the divergent tensor coefficients for massless particles including pentagons of rank 4 has been created with this purpose. This allows us to obtain also the terms of eq. (2.12) and the divergent parts of eq. (2.11) analytically up to this level.

It is known that the IR divergences depend on the kinematics of the external particles involved in the process, i.e., whether they are massless/massive on-shell/off-shell particles. Nevertheless, since we reconstruct the divergences numerically, to compute generally the amplitude of a particular diagram for a given helicity, τ, it is sufficient to consider off-shell vector bosons, V_i in figure 2. This basically means that all p_i^2 terms are kept and the transversality property of the vector on-shell bosons ($\epsilon(p_x)\cdot p_x = 0$) is not applied analytically, allowing us, the latter, to perform gauge tests ($\epsilon(p_x) \to p_x$) for on-shell massive particles. We note here that the polarization vectors can be understood as generic effective currents, $\epsilon^\mu(p_x) \to J^\mu_{\text{eff}}(p_x)$, which can include the leptonic decay of the vector bosons or physics BSM. Thus, denoted by $\mathcal{M}_{V_1V_2V_3V_4}$ the amplitude of the first diagram of figure 2 would be given by,

$$\mathcal{M}_{V_1V_2V_3V_4,\tau} = g_\tau^{V_1 f} g_\tau^{V_2 f} g_\tau^{V_3 f} g_\tau^{V_4 f} \frac{g_0^2}{(4\pi)^2} \mathcal{C}_{ij}^{V_1V_2V_3V_4} \mathcal{M}_\tau^{ij}, \tag{2.13}$$

where g_0 is the strong unrenormalized coupling, $\mathcal{M}_\tau^{ij}$ is the corresponding diagram with off-shell vector bosons (or effective currents) with color indices ij and given in terms of eq. (2.6) which is computed only once and for all vector bosons, $V_i \in (\gamma, W, Z, g)$. $\mathcal{C}_{ij}^{V_1V_2V_3V_4}$ is a color diagram dependent factor, e.g., $\mathcal{C}_{ij}^{\gamma\gamma g\gamma} = (T_a)_{ij}(C_F - 1/2C_A)$ and from now on the color sub-indices will be omitted. $g_\tau^{V_i f}$ is the coupling following the notation of ref. [87] with e.g., $g_\pm^{\gamma f} = |e|Q_f$, $g_-^{W f} = |e|/(\sqrt{2}\sin\theta_w)$, $g_-^{Z f} = |e|(T_{3f} - Q_f \sin^2\theta_w)/(\sin\theta_w \cos\theta_w)$, where θ_W is the weak mixing angle, T_{3f} is the third component of the isospin of the (left-handed) fermions, and $|e|$ the electric charge.

JHEP10(2011)070

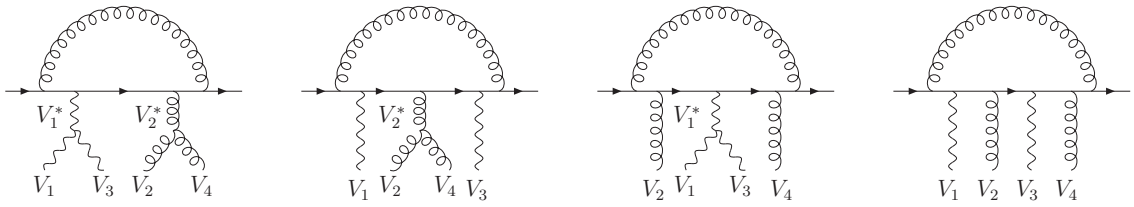

Figure 3. "Bosonic" one loop QED-like topologies appearing in the calculation of the virtual contributions for $pp \to VVjj + X$ production, with V$\in$ (W $^{\pm}$,Z,γ).

This procedure is advantageous for several reasons. First, when considering off-shell vector bosons, for example, diagrams with the same QED-like topology as the first one of figure 2 will give us, already, all the corrections needed for EW quadruple vector boson production, $pp \to VVVV + X$ and part of the $pp \to VVVj + X$ and $pp \to VVjj + X$ contributions, independently whether we are considering massless or massive particles or the bosons emitted from the quark line are gluons. $\mathcal{C}_{ij}^{V_1V_2V_3V_4}$ will associate the correct color factor to each diagram depending whether one is considering $pp \to VVVV + X$, $pp \to VVVj + X$ or $pp \to VVjj + X$ and $g_\tau^{V_i f}$ the corresponding couplings. Also, the leptonic decay of the vector bosons and new physic effects can be immediately incorporated by using the appropriate effective currents. Second, cross term related diagrams are obtained from the same analytical amplitude just by permuting the vector boson momenta and polarization, and thus, e.g., from the 24 cross related diagrams to the first one of figure 2, only the permutation depicted has to be computed. Moreover, additional checks can be implemented, as for example the factorization of the IR divergences against the born amplitude for different processes starting from the same analytical structure. In the following, we will refer to the first topology of figure 2 as contributions to $pp \to VVVV + X$ and, to the second as "bosonic" contributions to $pp \to VVVj + X$ since they appear for the first time in these processes.

2.1 Contributions to $pp \to VVVV + X$

In this section, all the "bosonic" QED-like loop corrections along a quark line needed for $pp \to VVjj + X$ production are considered. These contributions can be classified by **I)** virtual corrections along a quark line with two vector bosons attached (first diagram of figure 3) **II)** virtual corrections with three vector bosons attached to the quark line (second and third diagrams of figure 3) and **III)** virtual corrections along a quark line with four vector bosons attached (last diagram of figure 3). The strategy followed is to search for a minimal set of universal building blocks from which every amplitude can be constructed. We use the effective current approach described and applied in refs. [12, 15, 16, 89–93]. As illustration, the first diagram of figure 3 is used. This can be written as,

$$A_{V_1V_2V_3V_4,\tau} = J^{\mu_1}_{V_1^*} J^{\mu_2}_{V_2^*} \mathcal{M}_{\mu_1\mu_2,\tau} \equiv \mathcal{M}_{V_1^*V_2^*,\tau}, \tag{2.14}$$

where the color indices have been omitted. Here, $J^{\mu_1}_{V_1^*}$ and $J^{\mu_2}_{V_2^*}$ represent effective polarization vectors in the unitarity gauge for the EW sector including finite width effects in the

JHEP10(2011)070

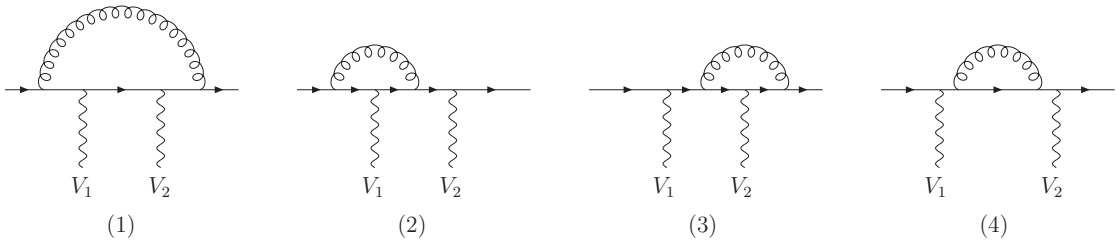

Figure 4. Virtual corrections for a fermion line with two vector bosons attached, $V_1(k_1)$ and $V_2(k_2)$ in a given permutation. The sum of these graphs defines $\mathcal{M}_{V_1V_2,\tau}$ in eq. (2.17).

scheme of refs. [17, 94] and propagator factors, e.g.,

$$J^{\mu_1}_{V_1^*}(q_1) = \frac{-i}{q_1^2 - M^2_{V_1^*} - i\, M_{V_1^*}\Gamma_{V_1^*}} \left(g^{\mu_1}_{\mu} - \frac{q_1^{\mu_1} q_{1\mu}}{q_1^2 - M^2_{V_1^*} - i\, M_{V_1^*}\Gamma_{V_1^*}} \right) \Gamma^{\mu}_{V_1^* V_1 V_3} \tag{2.15}$$

with $\Gamma_{V_1^*}$, the width of the V_1^* vector boson, and $\Gamma^{\mu}_{V_1^* V_1 V_3}$, the triple vertex which can also contain the leptonic decay of the EW vector bosons including all off-shell effects or BSM physics. In this manner, we can treat diagrams with triple vertexes as external off-shell legs (in the sense that they will have the same IR behavior). We can then concentrate in computing, instead of $A_{V_1V_2V_3V_4,\tau}$, the virtual correction to two massive vector bosons attached to the quark line, $\mathcal{M}_{V_1^*V_2^*,\tau}$, or equivalently $\mathcal{M}_{\mu_1\mu_2,\tau}$, where the polarization vectors or effective currents have been factored out. Thus, the strategy will be to combine in groups all the virtual corrections to a given born-amplitude configuration, independently of the effective currents or polarization vectors attached to the quark line. Furthermore, the order of the gauge bosons are fixed and the full amplitude will be recovered by summing over the physically-allowed permutations. Thus, three universal virtual contributions are left, corrections to a born amplitude with two, three and four vector bosons attached to the quark line for a given order permutation.

I) The virtual corrections to the Feynman graph with two vector bosons V_1 and V_2 attached to the quark line for a given order-permutation with incoming momenta k_1 and k_2 are depicted in figure 4 with kinematics,

$$q(p_1) + \bar{q}(p_2) + V_1(k_1) + V_2(k_2) \to 0. \tag{2.16}$$

The sum of the four amplitudes with a given helicity is written in terms of,

$$\begin{aligned}
\mathcal{M}_{V_1V_2,\tau} &= g^{V_1 f}_{\tau} g^{V_2 f}_{\tau} \frac{g_0^2}{(4\pi)^2} \sum_{n=1}^{4} \mathcal{C}^{V_1V_2}_{(n)} \mathcal{M}^{(n)}_{V_1V_2,\tau}\,, \\
\mathcal{M}^{(n)}_{V_1V_2,\tau} &= \widetilde{\mathcal{M}}^{(n)}_{V_1V_2,\tau} + \widetilde{\mathcal{N}}^{(n)}_{V_1V_2,\tau} + \frac{\mathcal{N}^{1,(n)}_{V_1V_2,\tau}}{\epsilon} + \sum_{i=1}^{2} \frac{\mathcal{M}^{i,(n)}_{V_1V_2,\tau}}{\epsilon^i},
\end{aligned} \tag{2.17}$$

where $\mathcal{M}_{V_1V_2,\tau}$ is called from now on "boxline" contribution. Although, we are interested on off-shell vector bosons emitted from the quark line (effective polarization vectors), the

JHEP10(2011)070

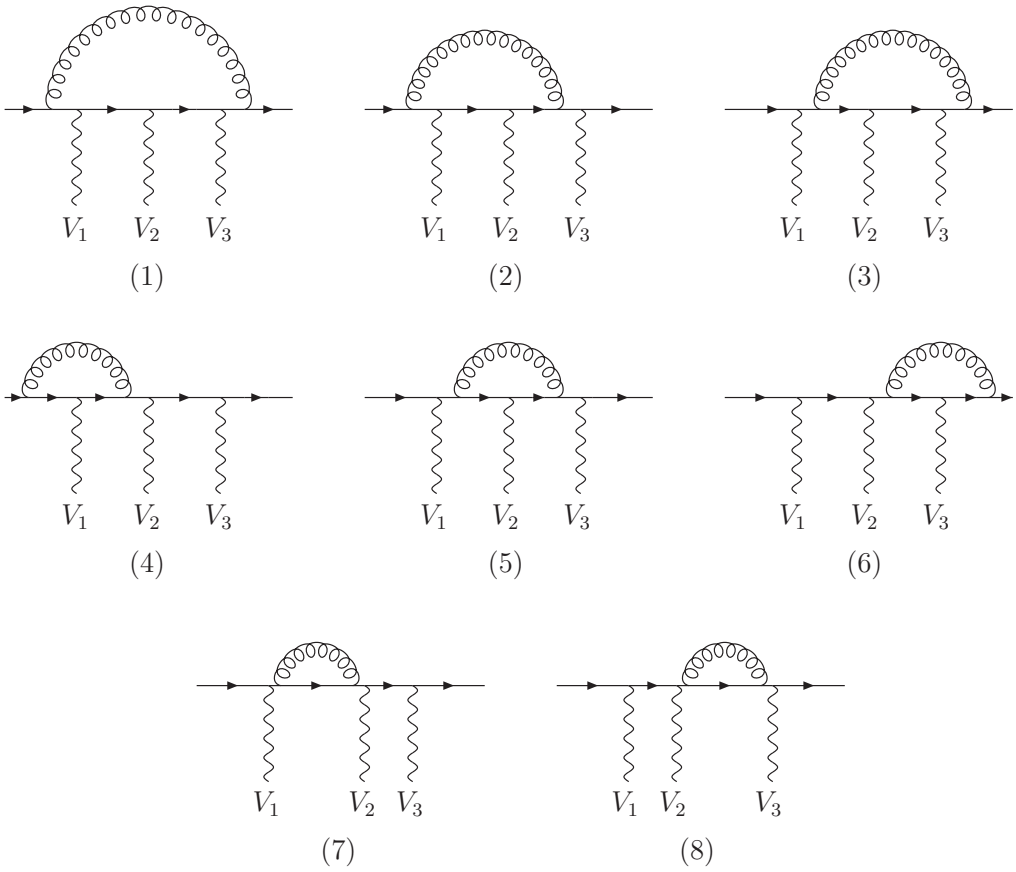

Figure 5. Virtual corrections for a fermion line with three vector bosons attached in a given permutation. The sum of these graphs defines $\mathcal{M}_{V_1V_2V_3,\tau}$ in eq. (2.19).

divergent contributions and $\widetilde{\mathcal{N}}^{(n)}_{V_1V_2,\tau}$ were also computed analytically for the different kinematic configurations. These configurations are obtained by considering the vector bosons massless or massive and all possible ordering permutations, i.e., $(k_1^2=0, k_2^2=0)$, $(k_1^2=M_1, k_2^2=0)$, $(k_1^2=0, k_2^2=M_2)$, $(k_1^2=M_1, k_2^2=M_2)$. From the analytical calculation, it is confirmed that the rational terms arise from diagrams with ultraviolet divergences, thus, $\widetilde{\mathcal{N}}^{(1)}_{V_1V_2,\tau}$ is zero. For configurations with massless vector bosons, $k_i^2=0$, the transversality property of the bosons must be used, $k_i\cdot\epsilon(k_i)=0$. A general proof of this statement was presented in ref. [88]. Moreover, $\mathcal{N}^{1,(n)}_{V_1V_2,\tau}$ is zero since there are not $1/\epsilon^2$ UV poles. For the self-energy diagram, $\mathcal{M}^{2,(4)}_{V_1V_2,\tau}$=0 since the divergences are only $1/\epsilon$. Finally, for $\mathcal{M}^{2,(2-3)}_{V_1V_2,\tau}$, there are not collinear and soft singularities simultaneously given rise to $1/\epsilon^2$ poles, so that, $\mathcal{M}^{2,(2-3)}_{V_1V_2,\tau}$=0.

II) The virtual corrections to the Feynman graph with three vector bosons V_1, V_2 and V_3 attached to the quark line for a given permutation are depicted in figure 5 with kinematics,

$$q(p_1)+\bar{q}(p_2)+V_1(k_1)+V_2(k_2)+V_3(k_3)\to 0. \tag{2.18}$$

JHEP10(2011)070

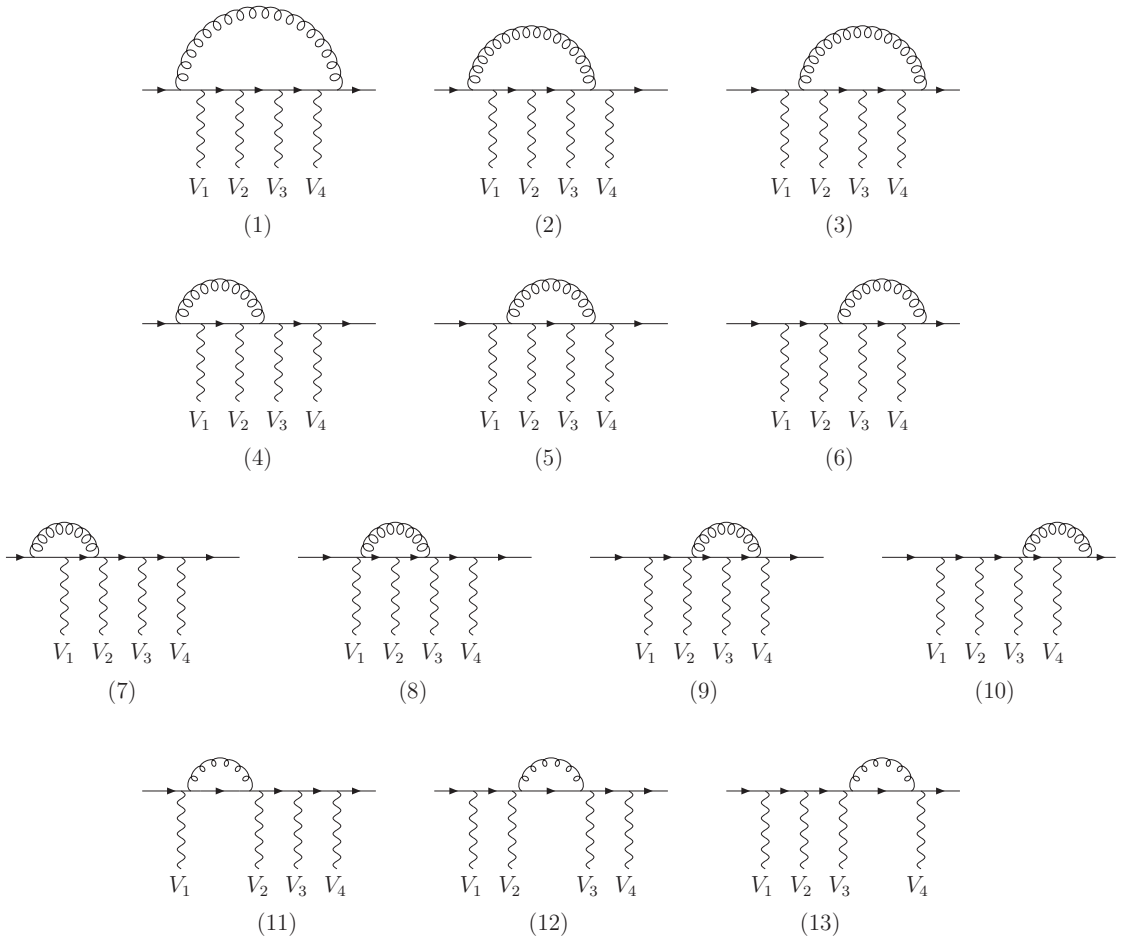

Figure 6. Virtual corrections for a fermion line with four vector bosons attached for a given order permutation. The sum of these graphs defines $\mathcal{M}_{V_1V_2V_3V_4,\tau}$ in eq. (2.21).

The sum of the eight diagrams with a given helicity is written in terms of,

$$\begin{aligned}\mathcal{M}_{V_1V_2V_3,\tau} &= g_\tau^{V_1 f} g_\tau^{V_2 f} g_\tau^{V_3 f} \frac{g_0^2}{(4\pi)^2} \sum_{n=1}^{8} \mathcal{C}_{(n)}^{V_1V_2V_3} \mathcal{M}_{V_1V_2V_3,\tau}^{(n)}\,,\\ \mathcal{M}_{V_1V_2V_3,\tau}^{(n)} &= \widetilde{\mathcal{M}}_{V_1V_2V_3,\tau}^{(n)} + \widetilde{\mathcal{N}}_{V_1V_2V_3,\tau}^{(n)} + \frac{\mathcal{N}_{V_1V_2V_3,\tau}^{1,(n)}}{\epsilon} + \sum_{i=1}^{2} \frac{\mathcal{M}_{V_1V_2V_3,\tau}^{i,(n)}}{\epsilon^i},\end{aligned} \tag{2.19}$$

where $\mathcal{M}_{V_1V_2V_3,\tau}$ is called from now on "penline" contribution. We have computed also the divergent contributions and $\widetilde{\mathcal{N}}_{V_1V_2V_3,\tau}^{(n)}$ analytically for the eight different kinematic configurations, $(k_1^2=0, k_2^2=0, k_3^2=0)$, $(k_1^2=M_1, k_2^2=0, k_3^2=0)$, $(k_1^2=M_1, k_2^2=M_2, k_3^2=0), \ldots$. From the analytical calculation, it is verified that once the transversality property for massless on-shell particles is applied, the rational terms arise from diagrams with ultraviolet divergences. Therefore, $\widetilde{\mathcal{N}}_{V_1V_2V_3,\tau}^{(1,2,3)}$ and $\mathcal{N}_{V_1V_2V_3,\tau}^{1,(n)}$ are zero. Analogously to the boxline, for self-energies, $\mathcal{M}_{V_1V_2V_3,\tau}^{2,(7,8)}$=0 as well as $\mathcal{M}_{V_1V_2V_3,\tau}^{2,(2-6)}$=0.

JHEP10(2011)070

III) The virtual corrections to the Feynman graph with four vector bosons V_1, V_2, V_3 and V_4 attached to the quark line for a given permutation are depicted in figure 6 with kinematics,

$$q(p_1) + \bar{q}(p_2) + V_1(k_1) + V_2(k_2) + V_3(k_3) + V_4(k_4) \to 0. \tag{2.20}$$

The sum of the thirteen diagrams with a given helicity is written in terms of,

$$\begin{aligned}
\mathcal{M}_{V_1V_2V_3V_4,\tau} &= g_\tau^{V_1 f} g_\tau^{V_2 f} g_\tau^{V_3 f} g_\tau^{V_4 f} \frac{g_0^2}{(4\pi)^2} \sum_{n=1}^{13} \mathcal{C}_{(n)}^{V_1V_2V_3V_4} \mathcal{M}^{(n)}_{V_1V_2V_3V_4,\tau}\,, \\
\mathcal{M}^{(n)}_{V_1V_2V_3V_4,\tau} &= \widetilde{\mathcal{M}}^{(n)}_{V_1V_2V_3V_4,\tau} + \widetilde{\mathcal{N}}^{(n)}_{V_1V_2V_3V_4,\tau} + \frac{\mathcal{N}^{1,(n)}_{V_1V_2V_3V_4,\tau}}{\epsilon} + \sum_{i=1}^{2} \frac{\mathcal{M}^{i,(n)}_{V_1V_2V_3V_4,\tau}}{\epsilon^i},
\end{aligned} \tag{2.21}$$

$\mathcal{M}_{V_1V_2V_3V_4,\tau}$ will be called "hexline" contribution in the following. For the hexline contribution, the divergences are not computed analytically. The explicit and naive recursive reduction and simplification of the tensor integrals for hexagons in terms of $1/\epsilon$ poles exceeds the capacity of Mathematica with 4 GB of memory RAM. Therefore, eqs. (2.11), (2.12) are used to obtain numerically the different contributions both at the Mathematica and FORTRAN level. We have checked with up to 30000 digits of precision in Mathematica for the 16 different kinematic configurations, i.e., $(k_1^2 = 0, k_2^2 = 0, k_3^2 = 0, k_4^2 = 0)$, $(k_1^2 = M_1, k_2^2 = 0, k_3^2 = 0, k_4^2 = 0)$, $(k_1^2 = M_1, k_2^2 = M_2, k_3^2 = 0, k_4^2 = 0), \ldots$ and several phase space points that $\widetilde{\mathcal{N}}^{(1-6)}_{V_1V_2V_3V_4,\tau}$ is zero for all possible kinematic configurations (for massless particles the transversality property must be used) as well as $\mathcal{N}^{1,(n)}_{V_1V_2V_3V_4,\tau} = \mathcal{M}^{2,(2-13)}_{V_1V_2V_3V_4,\tau} = 0$. At the FORTRAN level for non-singular points, the proof works at the working precision level.

2.1.1 Checks

In this section, the tests performed in order to ensure the correctness of the calculation of the 1 loop diagrams/contributions are explained. We consider electroweak vector boson production $(V_1,V_2,V_3,V_4) \in (\mathrm{W}^\pm,\mathrm{Z},\gamma)$. Then, the color factor for all diagrams and contributions is proportional to C_F. This is enough to test not only the individual diagrams but also the different contributions. For electroweak vector bosons, the divergent terms for the boxline and penline are known analytically, the general form generalizes for n vector boson emission and reads,

$$\begin{aligned}
\mathcal{M}_{V_1\ldots V_n,\tau} &= g_\tau^{V_1 f} \ldots g_\tau^{V_n f} C_F \frac{\alpha_s(\mu)}{4\pi} \\
&+ \left(\widetilde{\mathcal{M}}_V + \left(\frac{4\pi\mu^2}{-s}\right)^\epsilon \Gamma(1+\epsilon) \left[-\frac{2}{\epsilon^2} - \frac{10-D}{2\epsilon} \right] \mathcal{M}^B_{V_1\ldots V_n,\tau} \right), \quad (V_i) \in (\mathrm{W}^\pm, \mathrm{Z}, \gamma)
\end{aligned} \tag{2.22}$$

where $\mathcal{M}^B_{V_1\ldots V_n,\tau}$ is the corresponding Born amplitude with helicity τ and s the square of the partonic center-of-mass energy. If we use $c_\Gamma(-s)$ in eq. (A.2) for the definition of the scalar and tensor integrals and $D = 4-2\epsilon$, then, the pre-factor $\left(\frac{4\pi}{-s}\right)^\epsilon \Gamma(1+\epsilon)$ of eq. (2.22) is reproduced and each of the terms of eq. (2.22) can be identified, for example, for the

JHEP10(2011)070

hexline contribution, eq. (2.21), with the different finite and pole terms as,

$$\sum_{n=1}^{13} \widetilde{\mathcal{M}}^{(n)}_{V_1V_2V_3V_4,\tau} = \widetilde{\mathcal{M}}_V, \qquad \sum_{n=1}^{13} \mathcal{M}^{1,(n)}_{V_1V_2V_3V_4,\tau} = -3\mathcal{M}^{B}_{V_1V_2V_3V_4,\tau},$$
$$\sum_{n=1}^{13} \mathcal{M}^{2,(n)}_{V_1V_2V_3V_4,\tau} = -2\mathcal{M}^{B}_{V_1V_2V_3V_4,\tau},$$
$$\sum_{n=1}^{13} \widetilde{\mathcal{N}}^{(n)}_{V_1V_2V_3V_4,\tau} = -\mathcal{M}^{B}_{V_1V_2V_3V_4,\tau}, \qquad \sum_{n=1}^{13} \widetilde{\mathcal{N}}^{1,(n)}_{V_1V_2V_3V_4,\tau} = 0. \tag{2.23}$$

These relations are very important for testing purposes. Note that the left hand quantities for each of the above lines are obtained numerically from the same analytical expression, eqs. (2.11), (2.12). They only differ in which terms of the $1/\epsilon^n$ expansion of the scalar and tensor integrals are used. Therefore, the numerical check of the factorization of the singularities and rational terms provides a strong check of the correctness of the finite terms $\widetilde{\mathcal{M}}^{(n)}_{V_1V_2V_3v_4,\tau}$. We have checked the factorization formula analytically for the boxline and penline contributions for all different kinematic configurations. To cast the singularities in this form for massless on-shell vector bosons, (γ), the transversality property of the particle must be used. Otherwise, additional singularities proportional to the product $k_i \cdot \epsilon(k_i)$ appear, with k_i the on-shell massless particle momentum. Thus, we have checked that the presence of additional massless particles does not introduce new singularities or new rational terms in agreement with ref. [88]. For the hexline contribution, we have checked numerically with high precision in Mathematica the factorization formula for the 16 different kinematic configurations and for different phase space points. The coefficients multiplying the poles of eq. (2.22) are obtained with up to 30000 digits of precision at least (at the FORTRAN level, for non-singular points, the proof works at the working precision level). Nevertheless, we will assume the result to be analytic due to the high precision achieved. An analytical proof can be obtained using the method described in ref. [95] which is not automatized within our approach.

Concerning the origin of the rational terms in eq. (2.22), we note that for electroweak boson production, the wave renormalization functions (WRF), which are zero in Dimensional Regularization for massless on-shell quarks, together with $\mathcal{M}_{V_1\ldots V_n,\tau}$ are UV finite. Therefore, all the divergences in eq. (2.22), after adding the WRF, become of IR origin including the terms containing the rational factor, $D/(2\epsilon)$, of UV origin. This is clear since the WRF are zero due to the cancellation of IR and UV poles. Treating the UV and IR divergences separately, one observes that the UV poles of the WRF cancel the rational terms of eq. (2.22) and only IR divergences remain (see also ref. [88]).

The factorization proof already provides an important check of the correctness of the calculation. We can use the factorization formula to perform an additional test. The factorization of $(-s)^{-\epsilon}$ from the scalar integrals introduces an additional dependence in $\widetilde{\mathcal{M}}_v$ on this variable. If we consider (-s) as an independent scale energy variable, $-s \equiv \mu_0$, and series expand $(\mu_0)^{-\epsilon}$ in ϵ in the second piece of eq. (2.22), we obtain a new finite term,

JHEP10(2011)070

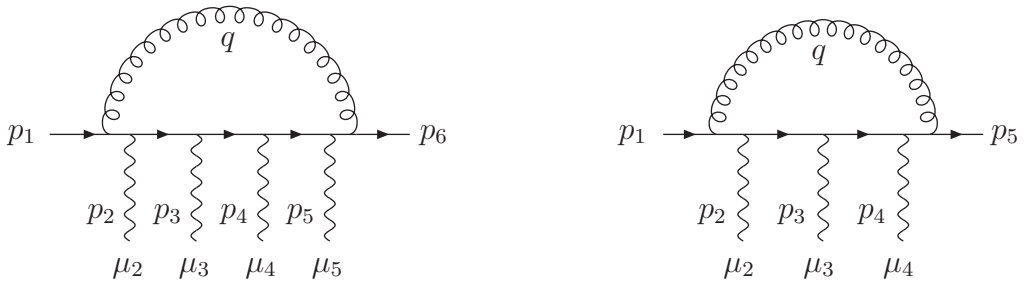

Figure 7. $\mathcal{F}_{\mu_2\mu_3\mu_4\mu_5}(p_1,p_2,p_3,p_4,p_5)$ and $\mathcal{E}_{\mu_2\mu_3\mu_4}(p_1,p_2,p_3,p_4)$ of eq. (2.25) and eq. (2.26).

$\widetilde{\mathcal{M}}'_V$, of the form,[3]

$$\widetilde{\mathcal{M}}'_V = \widetilde{\mathcal{M}}_V(\mu_0) + f(\mu_0)\cdot\mathcal{M}_B, \qquad \text{with} \qquad f(\mu_0) = -\left(\log^2(\mu_0) - 3\log(\mu_0)\right), \tag{2.24}$$

such that the $\log(\mu_0)$ terms compensate the μ_0 dependence propagated in all the scalar and tensor coefficient integrals in the complex $\widetilde{\mathcal{M}}_V(\mu_0)$. Thus, $\widetilde{\mathcal{M}}'_V$ is μ_0 independent. This fact was satisfied for non-singular points in the three contributions at the working precision level in the FORTRAN code (for the hexline contribution, see table 12) and at least with 30000 digits in the Mathematica code. Moreover, we have implemented Ward identity tests for the virtual corrections in FORTRAN and Mathematica at different levels of complexity:

1) At the level of single diagrams.

2) For the $\mathcal{M}_{V_1V_2,\tau}$, $\mathcal{M}_{V_1V_2V_3,\tau}$, $\mathcal{M}_{V_1V_2V_3V_4,\tau}$ contributions.

3) At the level of gauge invariant quantities.

4) Subset of amplitudes invariant for a specific replacement ($\epsilon(p_k)=\epsilon_k \to p_k$).

5) Specific contractions that make the contributions to vanish.

1) Under the replacement of the polarization vector by its momentum ($\epsilon(p_k) \to p_k$), relations among the different diagrams/topologies can be found. As illustration, one can consider the hexagon of figure 7,

$$\mathcal{F}_{\mu_2\mu_3\mu_4\mu_5}(p_1,p_2,p_3,p_4,p_5) = \int\frac{d^dq}{(2\pi)^d}\frac{1}{q^2}\gamma^\alpha\frac{1}{\not q+\not p_{15}}\gamma_{\mu_5}\frac{1}{\not q+\not p_{14}}\gamma_{\mu_4}\frac{1}{\not q+\not p_{13}}\gamma_{\mu_3}\frac{1}{\not q+\not p_{12}}\gamma_{\mu_2}\frac{1}{\not q+\not p_{1}}\gamma_\alpha \tag{2.25}$$

where $p_{1j}=\sum_{k=1}^{j}p_k$. Contracting one of the open indices by the corresponding momentum and expressing the contracted gamma matrix as the difference of two adjacent fermionic

[3]Note that $\widetilde{\mathcal{M}}_V(\mu_0)$ and $\widetilde{\mathcal{M}}'_V$, which is $\widetilde{\mathcal{M}}_V(\mu_0=1\text{GeV})$, have the same analytical structure. They only differ in the input scalar integrals.

JHEP10(2011)070

propagators, the hexagon is reduced to a difference of two pentagon integrals,

$$\begin{aligned}
p_2^{\mu_2}\mathcal{F}_{\mu_2\mu_3\mu_4\mu_5}(p_1,p_2,p_3,p_4,p_5) &= \mathcal{E}_{\mu_3\mu_4\mu_5}(p_1,p_2+p_3,p_4,p_5) - \mathcal{E}_{\mu_3\mu_4\mu_5}(p_1+p_2,p_3,p_4,p_5),\\
p_3^{\mu_3}\mathcal{F}_{\mu_2\mu_3\mu_4\mu_5}(p_1,p_2,p_3,p_4,p_5) &= \mathcal{E}_{\mu_2\mu_4\mu_5}(p_1,p_2,p_3+p_4,p_5) - \mathcal{E}_{\mu_2\mu_4\mu_5}(p_1,p_2+p_3,p_4,p_5),\\
p_4^{\mu_4}\mathcal{F}_{\mu_2\mu_3\mu_4\mu_5}(p_1,p_2,p_3,p_4,p_5) &= \mathcal{E}_{\mu_2\mu_3\mu_5}(p_1,p_2,p_3,p_4+p_5) - \mathcal{E}_{\mu_2\mu_3\mu_5}(p_1,p_2,p_3+p_4,p_5),\\
p_5^{\mu_5}\mathcal{F}_{\mu_2\mu_3\mu_4\mu_5}(p_1,p_2,p_3,p_4,p_5) &= \mathcal{E}_{\mu_2\mu_3\mu_4}(p_1,p_2,p_3,p_4) - \mathcal{E}_{\mu_2\mu_3\mu_4}(p_1,p_2,p_3,p_4+p_5).
\end{aligned} \tag{2.26}$$

where $\mathcal{E}_{\mu_i\mu_j\mu_k}$ represents the pentagon diagram of figure 7, defined similarly as eq. (2.25).

2) For the contributions, assuming EW vector boson production, equivalent relations can be obtained. First, we factor out the couplings and the polarization vectors,

$$\mathcal{M}_{V_1\ldots V_n,\tau}(p_1,\ldots,p_n) = g_\tau^{V_1 f}\ldots g_\tau^{V_n f}\epsilon_{V_1}^{\mu_2}(p_2)\ldots\epsilon_{V_n}^{\mu_n}(p_n)\mathcal{M}_{\mu_2\ldots\mu_n,\tau}(p_1,\ldots,p_n), \tag{2.27}$$

where $\mathcal{M}_{\mu_2\ldots\mu_n,\tau}(p_1,\ldots,p_n)$ represents the un-contracted contributions and we have explicitly written down the momentum's dependence following the convention of figure 7. Note that the color factors, $\mathcal{C}_{(m)}^{V_1\ldots V_n}$, are still present in $\mathcal{M}_{\mu_2\ldots\mu_n,\tau}(p_1,\ldots,p_n)$. Then, eq. (2.26) holds for the hexline and penline contributions with the replacements,

$$\begin{aligned}
\mathcal{F}_{\mu_2\mu_3\mu_4\mu_5} &\to \mathcal{M}_{\mu_2\mu_3\mu_4\mu_5,\tau},\\
\mathcal{E}_{\mu_i\mu_j\mu_l} &\to \mathcal{M}_{\mu_i\mu_j\mu_l,\tau}.
\end{aligned} \tag{2.28}$$

Analogously, the penline contribution can be checked against the boxline contribution obtaining similar relations. Additionally, to check the boxline contribution, we computed the quark line with one vector boson attached, which we called vertline, $\mathcal{M}_{\mu_2,\tau}$, and is formed by a simple vertex graph. These relations are satisfied independently both for the finite and the divergent parts of each contribution.

3) Vertline is gauge invariant under the replacement of $\epsilon^{\mu_i}(p_i) \to p_i^{\mu_i}$ which means that the equivalent form of eq. (2.26) gives zero. To build gauge invariant quantities for the other un-contracted contributions and for EW vector boson production, the cross diagrams must be considered[4] (See figure 8 as illustration). Thus, the sum of direct and cross terms under the replacement $\epsilon^{\mu_i}(p_i) \to p_i^{\mu_i}$ is gauge invariant:

$$\begin{aligned}
p_i^{\mu_i}\left(\mathcal{M}_{\mu_2\mu_3,\tau}(p_1,p_2,p_3) + \mathcal{M}_{\mu_3\mu_2,\tau}(p_1,p_3,p_2)\right) &= 0,\\
p_i^{\mu_i}\left(\mathcal{M}_{\mu_2\mu_3\mu_4,\tau}(p_1,p_2,p_3,p_4) + \mathcal{M}_{\mu_3\mu_2\mu_4,\tau}(p_1,p_3,p_2,p_4) + 4 \text{ other}\right) &= 0,\\
p_i^{\mu_i}\left(\mathcal{M}_{\mu_2\mu_3\mu_4\mu_5,\tau}(p_1,p_2,p_3,p_4,p_5) + \mathcal{M}_{\mu_3\mu_2\mu_4\mu_5,\tau}(p_1,p_3,p_2,p_4,p_5) + 22 \text{ other}\right) &= 0.
\end{aligned} \tag{2.29}$$

4) For the un-contracted penline and hexline and considering EW vector boson production, there are smaller subsets which give zero ("gauge invariant") for a given replacement ($\epsilon(p_k) \to p_k$). For the un-contracted penline $\mathcal{M}_{\mu_2\mu_3\mu_4,\tau}(p_1,p_2,p_3,p_4)$, a "gauge invariant"

[4]Note that for processes with W vector bosons not all the permutations are physically allowed.

JHEP10(2011)070

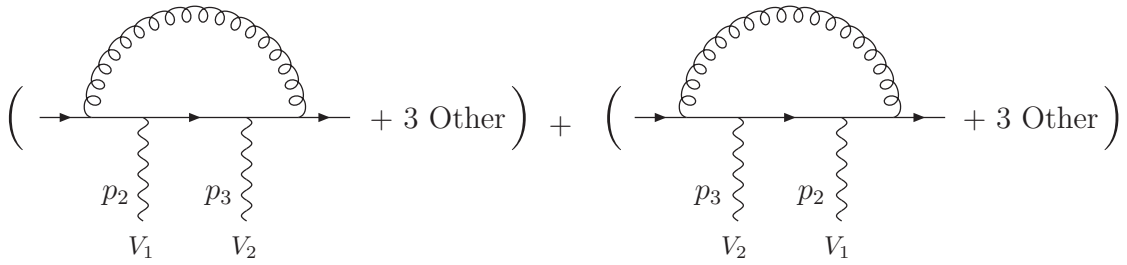

Figure 8. Direct and cross term diagrams which correspond to permuting the momenta and the polarization vectors in the boxline contributions yielding a gauge invariant subset for $V_i \in (\gamma, Z)$.

subset for a specific replacement, e.g., $\epsilon(p_2)^{\mu_2} \to p_2^{\mu_2}$ is obtained by permuting the position of the p_2 momentum and the corresponding Lorentz index and keeping the relative order of the other vector bosons fixed, i.e.,

$$p_2^{\mu_2}\left(\mathcal{M}_{\mu_2\mu_3\mu_4,\tau}(p_1,p_2,p_3,p_4)+\mathcal{M}_{\mu_3\mu_2\mu_4,\tau}(p_1,p_3,p_2,p_4)+\mathcal{M}_{\mu_3\mu_4\mu_2,\tau}(p_1,p_3,p_4,p_2)\right)=0. \tag{2.30}$$

The same can be proved performing the corresponding replacement $(\epsilon(p_k) \to p_k)$ for the contracted contributions which include the couplings $g_\tau^{V_n f}$, subject that $V_n \in (\gamma)$.

5) In addition, we have checked analytically and later on numerically that there are some combinations of replacements for the polarization vector which make for EW vector boson production the contributions to vanish. e.g.,

$$\begin{aligned}
(p_2^{\mu_2}(p_2+p_3)^{\mu_3}||(p_2+p_3)^{\mu_2}p_3^{\mu_3})\ \mathcal{M}_{\mu_2\mu_3,\tau}(p_1,p_2,p_3) &= 0,\\
p_2^{\mu_2}(p_2+p_3+p_4)^{\mu_3}p_4^{\mu_4}\ \mathcal{M}_{\mu_2\mu_3\mu_4,\tau}(p_1,p_2,p_3,p_4) &= 0,\\
(p_2^{\mu_2}(p_2+p_3)^{\mu_3}(p_2+p_3+p_4+p_5)^{\mu_3}p_5^{\mu_5}||p_2^{\mu_2}(p_2+p_3+p_4+p_5)^{\mu_3}(p_4+p_5)^{\mu_3}p_5^{\mu_5})&\\
\mathcal{M}_{\mu_2\mu_3\mu_4\mu_5,\tau}(p_1,p_2,p_3,p_4,p_5) &= 0.
\end{aligned} \tag{2.31}$$

The symbol || means throughout this paper that both contractions are possible. These tests have been implemented at the FORTRAN and Mathematica level. At the Mathematica level a precision of 30000 digits was achieved. At the FORTRAN level, for non-singular phase space points, these tests are satisfied at the working precision level. The finite boxline and penline contribution have essentially the same analytic expressions found in the calculation of the NLO QCD corrections in vector boson fusion processes, $qq \to Vqq$ and $qq \to VVqq$, discussed in refs. [17] and [18], respectively. We have checked that our results agree at the double precision level. The use of modular structure routines, as the above presented, has been proved to be an advantage in the program *VBFNLO* [96] since once a structure is computed and checked it can be reused for different processes. For example, the boxline and penline contributions computed here have been used to compute the NLQ QCD corrections to $W^\pm W^\pm Z$ [89], $W^+W^-\gamma$ $(ZZ\gamma)$ [90], $W^\pm Z\gamma$ [91], $W^\pm\gamma\gamma$ [92], $W^\pm\gamma jj$ [12, 16], $W^\pm Zj$ [15, 93] and also $H\gamma jj$ [97] production. They are publicly available as part of the *VBFNLO* package together with the tensor reduction routines up to the pentagon level, excluding the routines for small Gram determinants.

JHEP10(2011)070

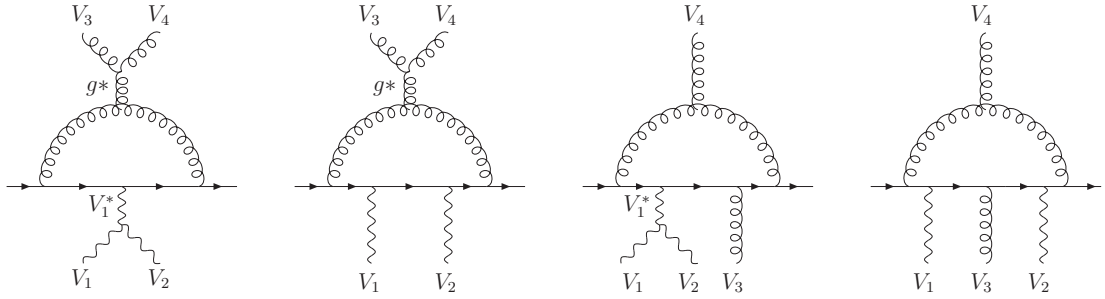

Figure 9. Topologies appearing in the calculation of the virtual contributions for $pp \to VVjj + X$ production, with V$\in$ (W $^{\pm}$,Z,γ) .

2.2 "Bosonic" contributions to $pp \to VVVj + X$

One loop non-abelian corrections involving one triple gluon vertex are considered in this section, figure 9. We follow the same strategy used in the previous section and classify the virtual corrections to three different groups depending whether they contribute to **I)** $q\bar{q}V_1^*g^* \to 0$, **II)** $q\bar{q}V_1V_2g^* \to 0$ or $q\bar{q}V_1^*V_3V_4 \to 0$ or **III)** $q\bar{q}V_1V_2V_3V_4 \to 0$. In analogy to the previous section, for the last two, only diagrams with a specific permutation of the vector bosons are considered. Generally, the momentum square for the off-shell legs V_1^* and g^*, indicated with a star, is not zero. This is important since it results in different IR divergences for individual graphs. From now on, to avoid confusion, the star is only kept for the gluon, but we remind the reader that at the programing level all vector bosons are considered to be off-shell as described in section 2 since the divergences are reproduced numerically, eqs. (2.11), (2.12).

I) Non-abelian corrections to the Feynman graphs with one vector boson V_1 attached to the quark line are depicted in figure 10 with kinematics,

$$q(p_1) + \bar{q}(p_2) + V_1(k_1) + g^*(k_2) \to 0. \tag{2.32}$$

The sum of the three graphs with a given helicity is written in terms of,

$$\begin{aligned}
\mathcal{M}^{g^*}_{V_1,\tau} &= g_\tau^{V_1 f} g_0 \frac{g_0^2}{(4\pi)^2} \sum_{n=1}^{3} \mathcal{C}^{g,V_1}_{(n)} \mathcal{M}^{g^*,(n)}_{V_1,\tau}, \\
\mathcal{M}^{g^*,(n)}_{V_1,\tau} &= \widetilde{\mathcal{M}}^{g^*,(n)}_{V_1,\tau} + \widetilde{\mathcal{N}}^{g^*,(n)}_{V_1,\tau} + \frac{\mathcal{N}^{g^*,1,(n)}_{V_1,\tau}}{\epsilon} + \sum_{i=1}^{2} \frac{\mathcal{M}^{g^*,i,(n)}_{V_1,\tau}}{\epsilon^i},
\end{aligned} \tag{2.33}$$

where $\mathcal{M}^{g^*}_{V_1,\tau}$ is called from now on "boxlineNoAbe" contribution. We have computed the divergent contributions and $\widetilde{\mathcal{N}}^{g^*,(n)}_{V_1,\tau}$ analytically for the 4 different kinematic configurations. From the analytical calculation using the transversality property for massless particles, it is confirmed that $\widetilde{\mathcal{N}}^{g^*,(1)}_{V_1,\tau}$ and $\mathcal{N}^{g^*,1,(n)}_{V_1,\tau}$ are zero.

II) The virtual corrections to the Feynman graph with two vector bosons V_1 and V_2 attached to the quark line for a given permutation are depicted in figure 11 with kinematics,

$$q(p_1) + \bar{q}(p_2) + V_1(k_1) + V_2(k_2) + g^*(k_3) \to 0. \tag{2.34}$$

JHEP10(2011)070

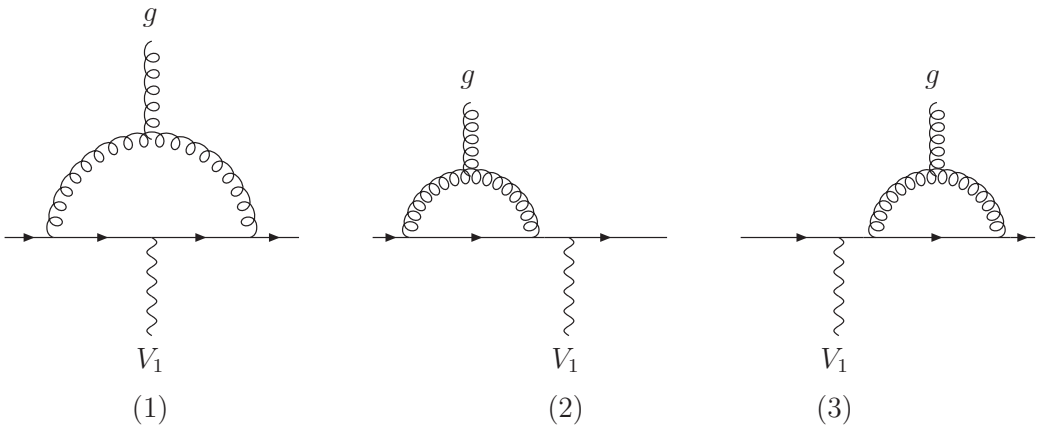

Figure 10. Virtual corrections for a fermion line with one vector boson attached, $V_1(k_1)$. The sum of these graphs defines $\mathcal{M}^{g^*}_{V_1,\tau}$ in eq. (2.33).

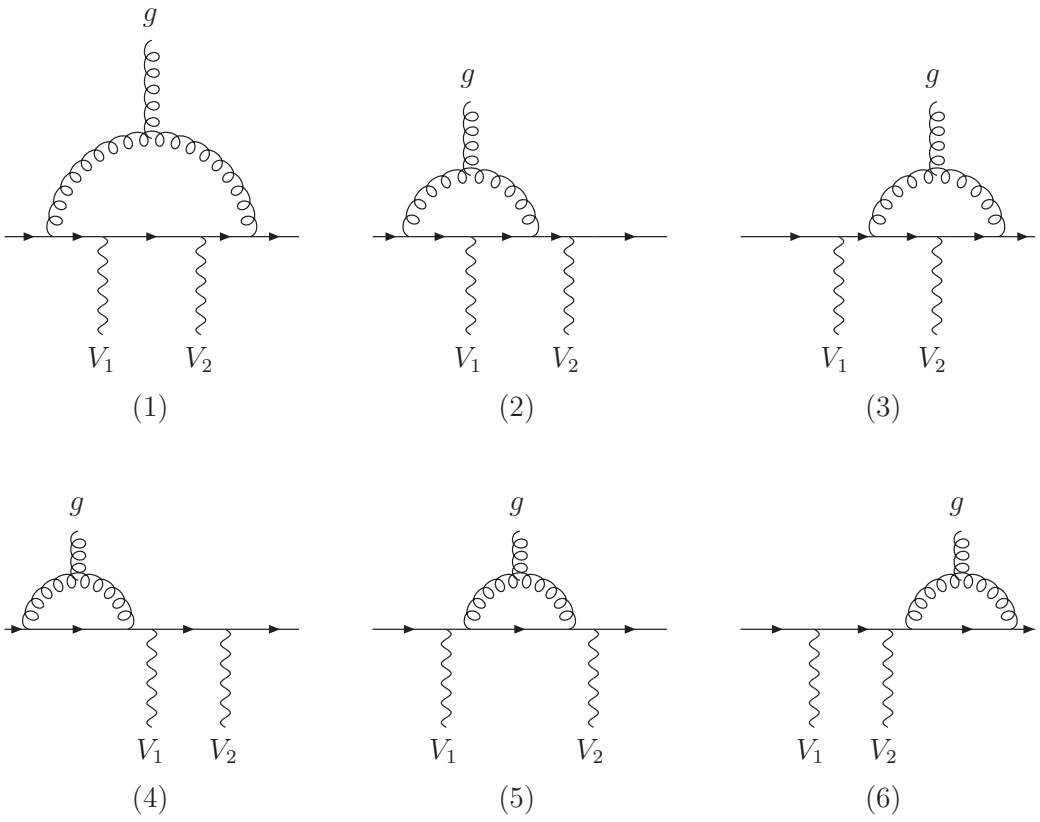

Figure 11. Virtual corrections for a fermion line with two vector bosons attached, $V_1(k_1)$ and $V_2(k_2)$ for a given order permutation. The sum of these graphs defines $\mathcal{M}^{g^*}_{V_1V_2,\tau}$ in eq. (2.35).

The sum of the six graphs with a given helicity is written in terms of:

$$\begin{aligned}\mathcal{M}^{g^*}_{V_1V_2,\tau} &= g_\tau^{V_1 f} g_\tau^{V_2 f} g_0 \frac{g_0^2}{(4\pi)^2} \sum_{n=1}^{6} \mathcal{C}_n^{g,V_1V_2} \mathcal{M}^{g^*,(n)}_{V_1V_2,\tau},\\ \mathcal{M}^{g^*,(n)}_{V_1V_2,\tau} &= \widetilde{\mathcal{M}}^{g^*,(n)}_{V_1V_2,\tau} + \widetilde{\mathcal{N}}^{g^*,(n)}_{V_1V_2,\tau} + \frac{\mathcal{N}^{g^*,1,(n)}_{V_1V_2,\tau}}{\epsilon} + \sum_{i=1}^{2} \frac{\mathcal{M}^{g^*,i,(n)}_{V_1V_2,\tau}}{\epsilon^i},\end{aligned} \tag{2.35}$$

JHEP10(2011)070

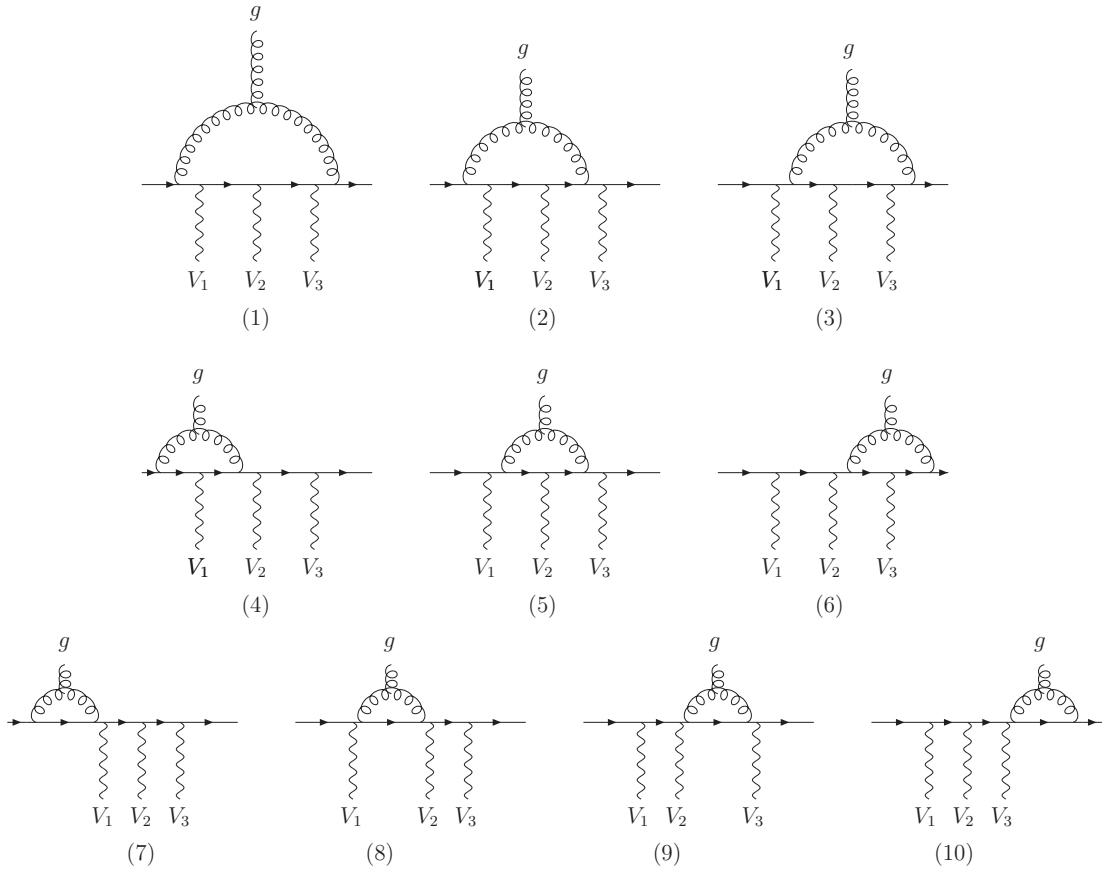

Figure 12. Virtual corrections for a fermion line with three vector bosons attached, $V_1(k_1)$, $V_2(k_2)$ and $V_3(k_3)$ for one permutation. The sum of these graphs defines $\mathcal{M}^{g^*}_{V_1V_2V_3,\tau}$ in eq. (2.37).

where $\mathcal{M}^{g^*}_{V_1V_2,\tau}$ is called "penlineNoAbe" contribution in the following. We have computed the divergent contributions and $\widetilde{\mathcal{N}}^{g^*,(n)}_{V_1V_2,\tau}$ analytically for the 8 different kinematic configurations. It is verified that $\widetilde{\mathcal{N}}^{g^*,(1-3)}_{V_1V_2,\tau}$ and $\mathcal{N}^{g^*,1,(n)}_{V_1V_2,\tau}$ are zero (the transversality property for massless particles must be used).

III) The virtual corrections to the Feynman graph with three vector bosons V_1, V_2 and V_3 attached to the quark line for a given permutation are depicted in figure 12 with kinematics,[5]

$$q(p_1) + \bar{q}(p_2) + V_1(k_1) + V_2(k_2) + V_3(k_3) + g^*(k_4) \to 0. \tag{2.36}$$

The sum of the ten diagrams with a given helicity is written in terms of:

$$\begin{aligned}
\mathcal{M}^{g^*}_{V_1V_2V_3,\tau} &= g_\tau^{V_1 f} g_\tau^{V_2 f} g_\tau^{V_3 f} g_0 \frac{g_0^2}{(4\pi)^2} \sum_{n=1}^{10} \mathcal{C}_n^{g,V_1V_2V_3} \mathcal{M}^{g^*,(n)}_{V_1V_2V_3,\tau} \,, \\
\mathcal{M}^{g^*,(n)}_{V_1V_2V_3,\tau} &= \widetilde{\mathcal{M}}^{g^*,(n)}_{V_1V_2V_3,\tau} + \widetilde{\mathcal{N}}^{g^*,(n)}_{V_1V_2V_3,\tau} + \frac{\mathcal{N}^{g^*,1,(n)}_{V_1V_2V_3,\tau}}{\epsilon} + \sum_{i=1}^{2} \frac{\mathcal{M}^{g^*,i,(n)}_{V_1V_2V_3,\tau}}{\epsilon^i},
\end{aligned} \tag{2.37}$$

[5]Note that we do not need to consider an off-shell gluon in this case since for $pp \to VVjj$ one of the V_i must be also a gluon in eq. (2.36).

JHEP10(2011)070

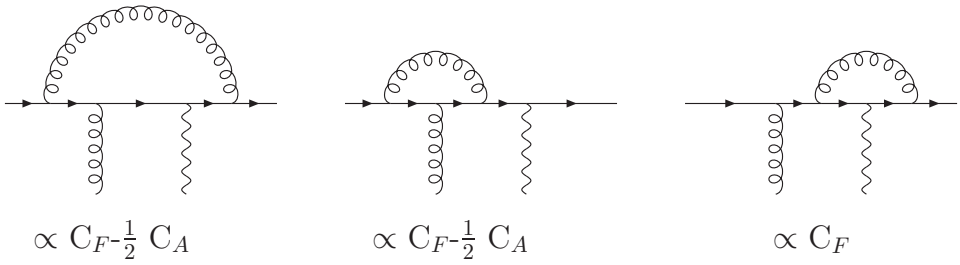

Figure 13. Color factors that appear when one gluon is emitted from the quark line.

$\mathcal{M}^{g^*}_{V_1V_2V_3,\tau}$ is called "hexlineNoAbe" contribution in the following. We have checked with high precision numerically in Mathematica that once the transversality property for massless particles is used, $\widetilde{\mathcal{N}}^{g^*(1-6)}_{V_1V_2V_3,\tau}$ and $\mathcal{N}^{g^*1,(n)}_{V_1V_2V_3,\tau}$ are zero for the 16 different kinematic configurations (at the FORTRAN level for non-singular points, this proof works at the working precision level).

2.2.1 Checks

The factorization of the infrared divergences for one or two electroweak vector boson production in association with one jet, $gu \to uV_1$ or $gu \to uV_1V_2$, is known analytically [12, 98]. We will make use of this fact to perform powerful tests to our contributions. For one gluon emission, the color for all the non-abelian contributions is proportional to C_A, and two color factors proportional to C_F and to $C_F - 1/2C_A$ (see figure 13) appear in the abelian contributions computed in the previous section. The relevant color factors for this proof for all diagrams of each abelian contribution are given in appendix C. We will concentrate in the hexline contributions since the penline and the boxline contributions are checked similarly. To verify the factorization of the divergences against the born amplitude for $(V_1, V_2, V_3) \in (W^\pm, Z, \gamma)$ and for an on-shell gluon, it is enough to consider all the diagrams mixed under the QCD gauge group for a given order combination of the vector bosons, (V_1, V_2, V_3),

$$\mathcal{M}_{gV_1V_2V_3,\tau} + \mathcal{M}_{V_1gV_2V_3,\tau} + \mathcal{M}_{V_1V_2gV_3,\tau} + \mathcal{M}_{V_1V_2V_3g,\tau} + \mathcal{M}^g_{V_1V_2V_3,\tau}. \tag{2.38}$$

The same is proved for the other six permutations ($V_1 \Leftrightarrow V_2 \Leftrightarrow V_3$). This combination under the replacement $\epsilon(k_4) \to k_4$, given the kinematics defined by eq. (2.36) is "gauge invariant". The virtual contributions factorize on the Born amplitude generalizing the result of diboson plus jet production. The sum of the amplitudes, including the counterterms (CT), in Dimensional Regularization are given by,

$$\begin{aligned}
&\mathcal{M}_{gV_1V_2V_3,\tau} + \mathcal{M}_{V_1gV_2V_3,\tau} + \mathcal{M}_{V_1V_2gV_3,\tau} + \mathcal{M}_{V_1V_2V_3g,\tau} + \mathcal{M}^g_{V_1V_2V_3,\tau} + CT = \\
&= \mathcal{M}^B_\tau \frac{\alpha_s(\mu^2)}{4\pi}\Gamma(1+\epsilon)\left\{\frac{1}{2}\left(\left(\frac{4\pi\mu^2}{-u}\right)^\epsilon + \left(\frac{4\pi\mu^2}{-t}\right)^\epsilon\right)\left(-\frac{C_A}{\epsilon^2} - \frac{\gamma_g}{\epsilon}\right)\right. \\
&\quad + \frac{1}{2}\frac{C_A}{C_F}\left(\left(\frac{4\pi\mu^2}{-u}\right)^\epsilon + \left(\frac{4\pi\mu^2}{-t}\right)^\epsilon - 2\left(\frac{4\pi\mu^2}{-s}\right)^\epsilon\right)\left(-\frac{C_F}{\epsilon^2} - \frac{\gamma_q}{\epsilon}\right) \\
&\quad \left. + 2\left(\frac{4\pi\mu^2}{-s}\right)^\epsilon\left(-\frac{C_F}{\epsilon^2} - \frac{\gamma_q}{\epsilon} + \frac{C_F(D-4)}{4\epsilon}\right)\right\} + \widetilde{\mathcal{M}}_V, \quad (V_1, V_2, V_3) \in (W^\pm, Z, \gamma),
\end{aligned} \tag{2.39}$$

JHEP10(2011)070

with

$$CT = -\mathcal{M}_\tau^B \frac{\alpha_s(\mu^2)}{4\pi}\Gamma(1+\epsilon)(4\pi)^\epsilon \frac{\gamma_g}{\epsilon}, \quad \gamma_q = \frac{3}{2}C_F, \quad \gamma_g = \frac{11}{6}C_A - \frac{2}{3}T_R N_f, \tag{2.40}$$

$T_R = 1/2$, $C_A = N$, and $C_F = (N^2-1)/(2N)$ in SU(N) gauge theory. The number of flavors is $N_f = 5$, s is the square of the partonic center-of-mass energy, $s = (p_1+p_2)^2$, $u = (p_1+k_4)^2$ and $t = (p_2+k_4)^2$, given the kinematics defined by eq. (2.36). $\mathcal{M}_\tau^B$ is the Born amplitude formed by four tree level graphs, the corresponding born amplitudes of each of the "hexline" contributions, $\mathcal{M}_\tau^B = \mathcal{M}^B_{V_1V_2V_3g\tau} + \mathcal{M}^B_{V_1V_2gV_3\tau} + \mathcal{M}^B_{V_1gV_2V_3\tau} + \mathcal{M}^B_{gV_1V_2V_3\tau}$. Given our definition for the scalar and tensor integrals, eq. (A.2), $\widetilde{\mathcal{M}}_V$ is defined through,

$$\begin{aligned}\sum_{n=1}^{13}\Bigg(&\mathcal{C}^{V_1V_2V_3g}_{(n)}\widetilde{\mathcal{M}}^{(n)}_{V_1V_2V_3g,\tau} + \mathcal{C}^{V_1V_2gV_3}_{(n)}\widetilde{\mathcal{M}}^{(n)}_{V_1V_2gV_3,\tau}\\ &+\mathcal{C}^{V_1gV_2V_3}_{(n)}\widetilde{\mathcal{M}}^{(n)}_{V_1gV_2V_3,\tau} + \mathcal{C}^{gV_1V_2V_3}_{(n)}\widetilde{\mathcal{M}}^{(n)}_{gV_1V_2V_3,\tau}\Bigg) +\\ &+\sum_{j=1}^{10}\mathcal{C}^{g,V_1V_2V_3}_{(j)}\widetilde{\mathcal{M}}^{g,(j)}_{V_1V_2V_3,\tau} = \widetilde{\mathcal{M}}_V + \mathcal{M}_\tau^B f(u,s,t,\mu^2,C_F,C_A,\gamma_g),\end{aligned} \tag{2.41}$$

where $f(u,s,t,\mu^2,C_F,C_A,\gamma_g)$ is given by the finite terms resulting of the epsilon expansion of eq. (2.39),

$$\begin{aligned}&f(u,s,t,\mu^2,C_F,C_A,\gamma_g)\\ &= -C_F\left(\log\left(\frac{-s}{\mu^2}\right) - \frac{2\gamma_q}{C_F}\right)\log\left(\frac{-s}{\mu^2}\right)\\ &\quad+\frac{\gamma_g}{2}\left(\log\left(\frac{-t}{\mu^2}\right)+\log\left(\frac{-u}{\mu^2}\right)\right) + C_A\left(\frac{1}{2}\left(\log^2\left(\frac{-s}{\mu^2}\right) - \log^2\left(\frac{-t}{\mu^2}\right) - \log^2\left(\frac{-u}{\mu^2}\right)\right)\right.\\ &\quad\left.+\frac{\gamma_g}{2C_F}\left(-2\log\left(\frac{-s}{\mu^2}\right)+\log\left(\frac{-t}{\mu^2}\right)+\log\left(\frac{-u}{\mu^2}\right)\right)\right).\end{aligned} \tag{2.42}$$

From the analytical form of the factorization formula, we can find relations for the divergent and rational terms. For the terms proportional to C_A, we get

$$\begin{aligned}&\frac{-1}{2}\Bigg(\sum_{n=1,3,6,10}\mathcal{M}^{1,(n)}_{V_1V_2V_3g,\tau} + \sum_{n=1-3,5,6,10}\mathcal{M}^{1,(n)}_{V_1V_2gV_3,\tau}\\ &\qquad+\sum_{n=1-5,8}\mathcal{M}^{1,(n)}_{V_1gV_2V_3,\tau} + \sum_{n=1,2,4,7}\mathcal{M}^{1,(n)}_{gV_1V_2V_3,\tau}\Bigg)\\ &\qquad\qquad+\sum_{j=1}^{10}\mathcal{M}^{g,1,(j)}_{V_1V_2V_3,\tau} = \mathcal{M}_\tau^B\left(-\log\left(\frac{-s}{\mu^2}\right)+\log\left(\frac{-t}{\mu^2}\right)+\log\left(\frac{-u}{\mu^2}\right)\right),\\ &\frac{-1}{2}\Bigg(\sum_{n=1,3,6,10}\mathcal{M}^{2,(n)}_{V_1V_2V_3g,\tau} + \sum_{n=1-3,5,6,10}\mathcal{M}^{2,(n)}_{V_1V_2gV_3,\tau}\\ &\qquad+\sum_{n=1-5,8}\mathcal{M}^{2,(n)}_{V_1gV_2V_3,\tau} + \sum_{n=1,2,4,7}\mathcal{M}^{2,(n)}_{gV_1V_2V_3,\tau}\Bigg) + \sum_{j=1}^{10}\mathcal{M}^{g,2,(j)}_{V_1V_2V_3,\tau} = -\mathcal{M}_\tau^B,\end{aligned}$$

JHEP10(2011)070

$$\frac{-1}{2}\Bigg(\sum_{n=1,3,6,10}\widetilde{\mathcal{N}}^{(n)}_{V_1V_2V_3g,\tau}+\sum_{n=1-3,5,6,10}\widetilde{\mathcal{N}}^{(n)}_{V_1V_2gV_3,\tau}$$
$$+\sum_{n=1-5,8}\widetilde{\mathcal{N}}^{(n)}_{V_1gV_2V_3,\tau}+\sum_{n=1,2,4,7}\widetilde{\mathcal{N}}^{(n)}_{gV_1V_2V_3,\tau}\Bigg)+\sum_{j=1}^{10}\widetilde{\mathcal{N}}^{g,(j)}_{V_1V_2V_3,\tau}=0,$$
$$\frac{-1}{2}\Bigg(\sum_{n=1,3,6,10}\mathcal{N}^{1,(n)}_{V_1V_2V_3g,\tau}+\sum_{n=1-3,5,6,10}\mathcal{N}^{1,(n)}_{V_1V_2gV_3,\tau}$$
$$+\sum_{n=1-5,8}\mathcal{N}^{1,(n)}_{V_1gV_2V_3,\tau}+\sum_{n=1,2,4,7}\mathcal{N}^{1,(n)}_{gV_1V_2V_3,\tau}\Bigg)+\sum_{j=1}^{10}\mathcal{N}^{g,2,(j)}_{V_1V_2V_3,\tau}=0, \quad (2.43)$$

and for the C_F terms,

$$\sum_{n=1}^{13}\left(\mathcal{M}^{1,(n)}_{V_1V_2V_3g,\tau}+\mathcal{M}^{1,(n)}_{V_1V_2gV_3,\tau}+\mathcal{M}^{1,(n)}_{V_1gV_2V_3,\tau}+\mathcal{M}^{1,(n)}_{gV_1V_2V_3,\tau}\right)=\mathcal{M}^B_\tau\left(-3+2\log\left(\frac{-s}{\mu^2}\right)\right),$$
$$\sum_{n=1}^{13}\left(\mathcal{M}^{2,(n)}_{V_1V_2V_3g,\tau}+\mathcal{M}^{2,(n)}_{V_1V_2gV_3,\tau}+\mathcal{M}^{2,(n)}_{V_1gV_2V_3,\tau}+\mathcal{M}^{2,(n)}_{gV_1V_2V_3,\tau}\right)=-2\mathcal{M}^B_\tau,$$
$$\sum_{n=1}^{13}\left(\widetilde{\mathcal{N}}^{(n)}_{V_1V_2V_3g,\tau}+\widetilde{\mathcal{N}}^{(n)}_{V_1V_2gV_3,\tau}+\widetilde{\mathcal{N}}^{(n)}_{V_1gV_2V_3,\tau}+\widetilde{\mathcal{N}}^{(n)}_{gV_1V_2V_3,\tau}\right)=-\mathcal{M}^B_\tau,$$
$$\sum_{n=1}^{13}\left(\mathcal{N}^{1,(n)}_{V_1V_2V_3g,\tau}+\mathcal{N}^{1,(n)}_{V_1V_2gV_3,\tau}+\mathcal{N}^{1,(n)}_{V_1gV_2V_3,\tau}+\mathcal{N}^{1,(n)}_{gV_1V_2V_3,\tau}\right)=0. \quad (2.44)$$

We have checked numerically with high precision in Mathematica the factorization formula for the 8 different kinematic configurations of the hexlines once $k_4^2=0$ is fixed, i.e., $(k_1^2=0,k_2^2=0,k_3^2=0,k_4^2=0)$, $(k_1^2=M_1,k_2^2=0,k_3^2=0,k_4^2=0)$, $(k_1^2=M_1,k_2^2=M_2,k_3^2=0,k_4^2=0),\ldots$. The coefficients multiplying the poles of eq. (2.39) are obtained with 30000 digits of precision at least (at the FORTRAN level for non-singular points, the proof works at the working precision level). The transversality property for the on-shell massless particles must be applied also in this case. For the penline and boxline contributions, similar relations are found. In addition, for them, we have checked the factorization formula analytically for all possible kinematic configurations, once the on-shellness of the gluon, $p_g^2=0$, is imposed.

As in the pure abelian case, the factorization of the divergences, for the sum of the $\mathcal{M}^{(i)}$ terms, against the born amplitude at the numerical and analytical level already provides a strong check of the correctness of the result since $\widetilde{\mathcal{M}}$ and $\mathcal{M}^{(i)}$ have the same analytical structure, eq. (2.11). The cancellation of the renormalization scale variable, μ, in $\widetilde{\mathcal{M}}_V$, eq. (2.41), provides an additional strong check (see table 17 for hexagons). Additionally, similar to the pure abelian case, we have implemented Ward identity tests for the virtual corrections in FORTRAN and Mathematica at different levels of complexity:

1) At the level of single diagrams.

2) For the different topologies $\mathcal{M}^{g^*}_{V_1,\tau}$, $\mathcal{M}^{g^*}_{V_1V_2,\tau}$ and $\mathcal{M}^{g^*}_{V_1V_2V_3,\tau}$.

JHEP10(2011)070

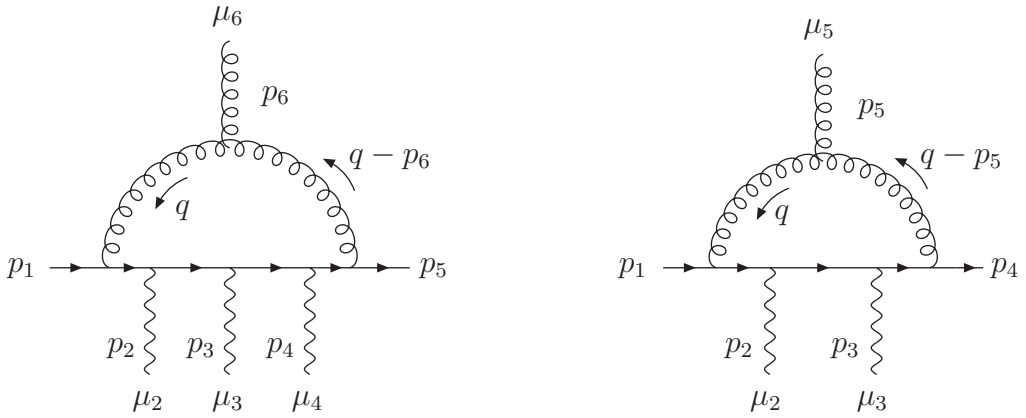

Figure 14. $\mathcal{F}^{g^*}_{\mu_2\mu_3\mu_4\mu_6}(p_1,p_2,p_3,p_4,p_5,p_6)$ and $\mathcal{E}^{g^*}_{\mu_2\mu_3\mu_5}(p_1,p_2,p_3,p_4,p_5)$ of eq. (2.45) and eq. (2.46).

3) At the level of gauge invariant amplitudes for one gluon emission.

4) Subset of amplitudes invariant for a specific replacement ($\epsilon(p_k) = \epsilon_k \to p_k$).

5) Specific contractions that make the contributions to vanish.

1) and 2) Under the replacement of the polarization vector by its momentum ($\epsilon(p_k) \to p_k$) for the EW vector bosons, relations among the different diagrams/contributions can be obtained. Considering the hexagon of figure 14,

$$\begin{aligned}&\mathcal{F}^{g^*}_{\mu_2\mu_3\mu_4\mu_6}(p_1,p_2,p_3,p_4,p_5,p_6) \\ &\quad= \int \frac{d^dq}{(2\pi)^d}\frac{1}{q^2}\frac{1}{(q-p_6)^2}\gamma_\alpha\frac{1}{\not{q}+\not{p}_{14}}\gamma_{\mu_4}\frac{1}{\not{q}+\not{p}_{13}}\gamma_{\mu_3}\frac{1}{\not{q}+\not{p}_{12}}\gamma_{\mu_2}\frac{1}{\not{q}+\not{p}_1}\gamma_\beta V^\alpha_{\mu_6}(q-p_6,p_6,q),\end{aligned} \tag{2.45}$$

with $V^\alpha_{\mu_6}(q-p_6,p_6,q)$, the triple gluon vertex. Note that we have kept the complete dependency of the momenta for clarity despite the fact that we can use momentum conservation to eliminate one of them. Then, contracting one of the open indices by the corresponding momentum and expressing the contracted gamma matrix as the difference of two adjacent fermionic propagators, we find the following relations,

$$\begin{aligned}&p_2^{\mu_2}\mathcal{F}^{g^*}_{\mu_2\mu_3\mu_4\mu_6}(p_1,p_2,p_3,p_4,p_5,p_6) \\ &\qquad= \mathcal{E}^{g^*}_{\mu_3\mu_4\mu_6}(p_1,p_2+p_3,p_4,p_5,p_6) - \mathcal{E}^{g^*}_{\mu_3\mu_4\mu_6}(p_1+p_2,p_3,p_4,p_5,p_6) \\ &p_3^{\mu_3}\mathcal{F}^{g^*}_{\mu_2\mu_3\mu_4\mu_6}(p_1,p_2,p_3,p_4,p_5,p_6) \\ &\qquad= \mathcal{E}^{g^*}_{\mu_2\mu_4\mu_6}(p_1,p_2,p_3+p_4,p_5,p_6) - \mathcal{E}^{g^*}_{\mu_2\mu_4\mu_6}(p_1,p_2+p_3,p_4,p_5,p_6) \\ &p_4^{\mu_4}\mathcal{F}^{g^*}_{\mu_2\mu_3\mu_4\mu_6}(p_1,p_2,p_3,p_4,p_5,p_6) \\ &\qquad= \mathcal{E}^{g^*}_{\mu_2\mu_3\mu_6}(p_1,p_2,p_3,p_4+p_5,p_6) - \mathcal{E}^{g^*}_{\mu_2\mu_3\mu_6}(p_1,p_2,p_3+p_4,p_5,p_6),\end{aligned} \tag{2.46}$$

where $\mathcal{E}^{g^*}_{\mu_1\mu_2\mu_3}$ represents the pentagon diagram of figure 14, defined similarly as eq. (2.45). For the contributions, $V_i \in (W^\pm, Z, \gamma)$ is considered such that only one global color factor

JHEP10(2011)070

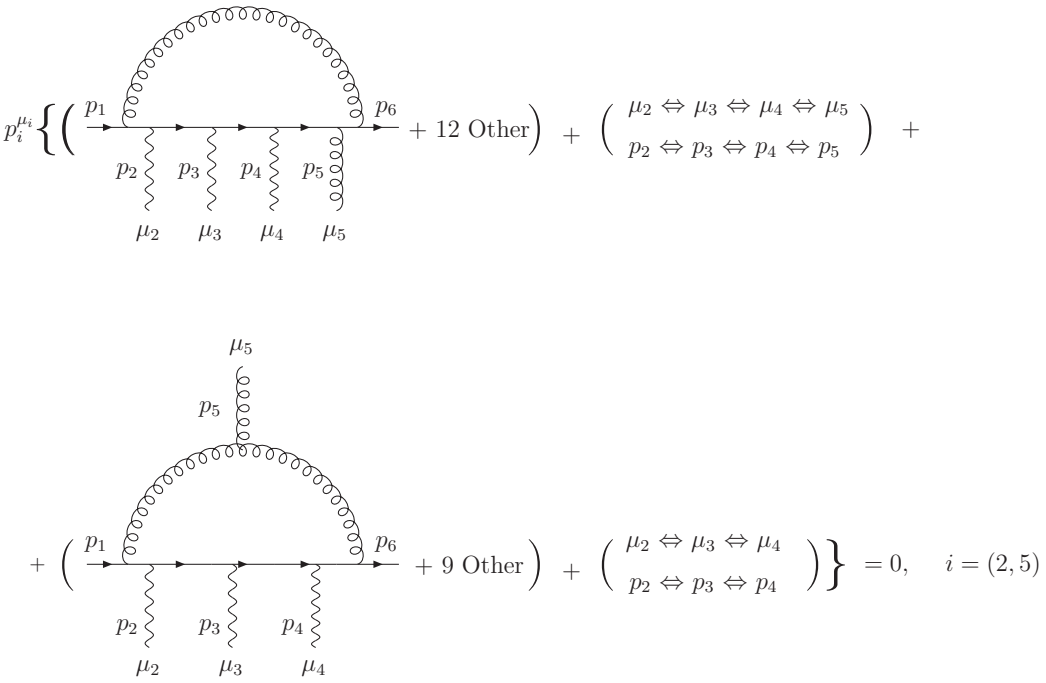

Figure 15. Direct and cross terms of eq. (2.21) and eq. (2.37) forming a gauge invariant quantity.

appears for all diagrams of figures 10, 11 and 12. Then, factorizing out the polarization vectors and couplings,

$$\mathcal{M}^{g^*}_{V_1\ldots V_n,\tau}(p_1,\ldots,p_{n+2}) = g_\tau^{V_1 f}\ldots g_\tau^{V_n f} g_0 \epsilon_{V_1}^{\mu_2}(p_2)\ldots\epsilon_{V_n}^{\mu_n}(p_n)\epsilon_g^{\mu_{n+2}}(p_{n+2})\mathcal{M}^{g^*}_{\mu_2\ldots\mu_n\mu_{n+2},\tau}(p_1,\ldots,p_{n+2}), \quad (2.47)$$

the same relation holds for the hexlineNoAbe and penlineNoAbe contributions under the replacements,

$$\begin{aligned}\mathcal{F}^{g^*}_{\mu_2\mu_3\mu_4\mu_6} &\to \mathcal{M}^{g^*}_{\mu_2\mu_3\mu_4\mu_6,\tau},\\ \mathcal{E}^{g^*}_{\mu_i\mu_j\mu_l} &\to \mathcal{M}^{g^*}_{\mu_i\mu_j\mu_l,\tau}.\end{aligned} \quad (2.48)$$

Similar relations are obtained between the penlineNoAbe and boxlineNoAbe contributions. Finally, the EW Ward Identity for the boxlineNoAbe routine returns directly zero.

3) To check gauge invariance for EW boson production with an additional jet and due to the fact that QCD mixes, for example, the topologies of the figures 6 and 12, we have to consider the abelian type contributions of the previous section, including the cross terms, along with the non-abelian type contributions[6] (see figure 15 for the convention of momenta and to illustration). For the different topologies, it is satisfied that

$$p_i^{\mu_i}\Big(\mathcal{M}_{\mu_2\mu_3,\tau}(p_1,p_2,p_3) + \mathcal{M}_{\mu_3\mu_2,\tau}(p_1,p_3,p_2) + \mathcal{M}^{g}_{\mu_2\mu_3,\tau}(p_1,p_2,p_4,p_3)\Big) = 0$$

[6]Note that for processes with W vector bosons not all the permutations are physically allowed.

JHEP10(2011)070

$$
\begin{aligned}
p_i^{\mu_i}\Big(&\mathcal{M}_{\mu_2\mu_3\mu_4,\tau}(p_1,p_2,p_3,p_4)+5\text{ other}\\
&+\mathcal{M}^g_{\mu_2\mu_3\mu_4,\tau}(p_1,p_2,p_3,p_5,p_4)+1\text{ other}\Big)=0\\
p_i^{\mu_i}\Big(&\mathcal{M}_{\mu_2\mu_3\mu_4\mu_5,\tau}(p_1,p_2,p_3,p_4,p_5)+23\text{ other}\\
&+\mathcal{M}^g_{\mu_3\mu_2\mu_4\mu_5,\tau}(p_1,p_3,p_2,p_4,p_6,p_5)+5\text{ other}\Big)=0.
\end{aligned}
\tag{2.49}
$$

The abelian contributions with an emitted gluon give rise to two different color structures, figure 13. The non-abelian type contributions are proportional to C_A and their contribution cancel in the gauge test eq. (2.49) against the abelian type ones proportional to C_A. The C_F terms from the abelian contribution cancel against themselves as discussed in the previous section, therefore, each one of the equalities of eq. (2.49) allow us to check on the one hand the abelian type contributions and, on the other hand, the interplay between the abelian and non-abelian contributions.

4) For penlineNoAbe and hexlineNoAbe contributions, there are as well "gauge invariant" subsets for an specific replacement. For example, for the hexline and hexlineNoAbe contributions with gluon momentum, p_5, an invariant subset under the replacement $\epsilon(p_5)\to p_5$ is obtained by permuting the position of the p_5 momentum and the corresponding Lorentz index and keeping the relative order of the other vector bosons fixed, i.e.,

$$
\begin{aligned}
p_5^{\mu_5}\,(&\mathcal{M}_{\mu_2\mu_3\mu_4\mu_5,\tau}(p_1,p_2,p_3,p_4,p_5)+\mathcal{M}_{\mu_2\mu_3\mu_5\mu_4,\tau}(p_1,p_2,p_3,p_5,p_4)+\\
&+\mathcal{M}_{\mu_2\mu_5\mu_3\mu_4,\tau}(p_1,p_2,p_5,p_3,p_4)+\mathcal{M}_{\mu_5\mu_2\mu_3\mu_4,\tau}(p_1,p_5,p_2,p_3,p_4)+\\
&+\mathcal{M}^g_{\mu_2\mu_3\mu_4\mu_5,\tau}(p_1,p_2,p_3,p_4,p_6,p_5))=0.
\end{aligned}
\tag{2.50}
$$

Note also that the divergences of this combination also factorize to the born amplitude, eq. (2.38).

5) In addition, we have checked analytically and later on numerically that there are some combinations of replacements for the polarization vectors which make the contributions to vanish,

$$
\begin{aligned}
(p_2^{\mu_2})\;\;\mathcal{M}^g_{\mu_2\mu_4,\tau}(p_1,p_2,p_3,p_4)&=0,\\
(p_2^{\mu_2}(p_2+p_3)^{\mu_3}||(p_2+p_3)^{\mu_2}p_3^{\mu_3})\;\;\mathcal{M}^g_{\mu_2\mu_3\mu_5,\tau}(p_1,p_2,p_3,p_4,p_5)&=0,\\
p_2^{\mu_2}(p_2+p_3+p_4)^{\mu_3}p_4^{\mu_4}\mathcal{M}^g_{\mu_2\mu_3\mu_4\mu_6,\tau}(p_1,p_2,p_3,p_4,p_5,p_6)&=0.
\end{aligned}
\tag{2.51}
$$

Note that the first line represents the EW Ward identity for the boxlineNoAbe, equivalent to eq. (2.46), which is zero as mentioned previously.

3 Numerical instabilities and timing

To study the stability and timing of the contributions computed here, we have used $5\cdot 10^5$ cut-accepted points for the vector boson fusion process $qq\to qqW^+W^-$ at LO generated with *VBFNLO* [96] applying the cuts,

$$
p_{Tj}\geq 20\;\text{Gev},\;\;|y_j|\leq 4.5,\;\;\Delta y_{jj}>4,
\tag{3.1}
$$

JHEP10(2011)070

Functions	SM's	F1's	F's
Recalculate for different spinor helicity	Yes	No	No
Recalculate for different polarization vector ($\epsilon(p_i) \to p_i$, $\epsilon_+(p_i) \to \epsilon_-(p_i)$	Yes	Yes	No
%CPU/Total	$\approx 1\%$	$\approx 30\%$	$\approx 70\%$

Table 1. CPU time to revaluate different parts of the code under changes of spinor helicities and polarization vectors for the hexline contribution.

p_{Tj} and $|y_j|$ are the transverse momentum and rapidity of the jets, respectively. Δy_{jj} is the tagging jet rapidity separation. Furthermore, we require the two tagging jets to lay in opposite detector hemispheres,

$$y_{j1} \times y_{j2} < 0, \tag{3.2}$$

with an invariant mass of $M_{jj} > 600$GeV. For the hexline(NoAbe) contribution, we assign the momenta of the two outgoing jets to two of the vector bosons emitted from the quark line in figure 6 (figure 12). The corresponding polarization vectors are constructed following the conventions of ref. [99] (eq. (A.11) of that paper). For the boxline(NoAbe) and penline(NoAbe) contributions, the momenta of the external particles are combined to obtain $2 \to 3$ and $2 \to 2$ kinematics. Different combinations and/or permutations yield similar results, we show here the more unstable observed.

The contributions are written automatically into FORTRAN modular routines in which some flags are incorporated to take advantage of the structure of the result. Note that the information of the spinor helicity is contained in the matrix elements, $\mathrm{SM}_{i,\tau}$ (eq. (2.8)), which are computed following the helicity method. Thus, calling the routines with a different spinor helicity only requires to recalculate the reduced set of standard matrix elements $\mathrm{SM}_{i,\tau}$, which represents less than 1 % of the total CPU time for the hexline(NoAbe) contributions. Additionally, for changes on the vector bosons due to different helicities or to the implementation of gauge tests ($\epsilon(p_n) \to p_n$), only the $\mathrm{F1}_j$ and $\mathrm{SM}_{i,\tau}$ of eq. (2.8) should be recalculated, but not the F_k from eq. (2.9). In table 1, as an example, the summary of the CPU time spent to revaluate the different parts of the code, as well as the part of the code that has to be revaluated under changes of spinor helicities and polarization vectors, are shown for the hexline contribution.

The organization of the code in dependent/independent loop integral parts is of advantage since additional callings of the routines for making Ward identity gauge tests are obtained at a lower CPU time cost. To control the stability of our routines for the finite terms of each of the contributions (boxline(NoAbe), penline(NoAbe), hexline(NoAbe)), for every phase space point, all the possible Ward identity gauge tests ($\epsilon(p_j) \to p_j$) of eqs. (2.26), (2.46) are performed. Except for the boxlineNoAbe, which vanishes for the

JHEP10(2011)070

Test Accuracy	10^{-1}	10^{-2}	10^{-3}	10^{-4}	10^{-5}	10^{-6}
Failed points for Boxline	0.002‰	0.008‰	0.01 ‰	0.05‰	0.1 ‰	0.4‰
Failed points for Penline	0.1‰	0.3‰	0.8‰	2 ‰	0.9 %	3.7 %
Failed points for Hexline	2‰	5‰	1.1%	2.8 %	7.6 %	18.1 %

Table 2. Fraction of unstable points, out of the sample of $5 \cdot 10^5$ events, depending on the accuracy of the gauge test for the abelian contributions eq. (2.17), eq. (2.19) and eq. (2.21).

Test Accuracy	10^{-1}	10^{-2}	10^{-3}	10^{-4}	10^{-5}	10^{-6}
Failed points for BoxlineNoAbe	0.008‰	0.03‰	0.07‰	0.2 ‰	0.6 ‰	1.8 ‰
Failed points for PenlineNoAbe	none	0.004‰	0.01‰	0.3 ‰	4.6 ‰	3.6 %
Failed points for HexlineNoAbe	0.5‰	1.2‰	4.1‰	1.4 %	4.4 %	12%

Table 3. Fraction of unstable points, out of the sample of $5 \cdot 10^5$ events, depending on the accuracy of the gauge test for the non-abelian contributions eq. (2.33), eq. (2.35) and eq. (2.37).

EW Ward identity gauge test of eq. (2.46), and eq. (2.49) is applied with the replacement $\epsilon(p_g) \to p_g$. These equations can be rewritten in the more convenient form "abs(a/b)-1=0" such that we obtain normalized results which allow us to test the accuracy of our numerical zeros, subject that there is not any numerical cancellation in the determination of the "a" and "b" quantity. In that case, we use "a-b=0". In practice, we take the worse normalized value of the Ward identity gauge test and compare it with a minimum accepted accuracy, i.e., abs(a/b)-1 < "accuracy". We define as unstable point the one that does not satisfy the Ward identity gauge test at a given accuracy. The factorization proof of the divergences to control the stability is not used since they need different input integrals (eq. (2.5)) and the complete routine has to be revaluated. The use of the Ward identities gauge test for the finite contributions has the additional advantage that the same integrals and tensor coefficients, stored in the F_j functions (eq. (2.9)), needed to provide the finite result, $\mathcal{M}_v$, are used. Moreover, since the rational terms and the poles will factorize against the born amplitude, we will not revaluate the routines for the poles (eqs. (2.11), (2.12)), but, instead, in practical implementations, we will use the analytical form which only requires to evaluate the born amplitude.

The fraction of unstable points for the different contributions depending on the accuracy of the Ward identity gauge tests can be seen in tables 2 and 3. For the determination of the tensor coefficients, we have applied the Passarino-Veltman tensor decomposition method following eqs. (A.7) and (A.7) up to the box level, and the Denner-Dittmaier method for pentagons and hexagons applying eqs. (A.12) and (A.13). To deal with these unstable points, some knowledge about the origin of these instabilities is required. It is known that small Gram determinants appearing in C and D functions and small Cayley determinants for E and F functions result in a loss of precision in the determination of the tensor coefficient integrals, therefore, in the amplitudes. To solve this problem within double precision accuracy, we try to improve the determination of the tensor coefficients up to the box level. First, using a fast implementation of the LU decomposition method (LU)

JHEP10(2011)070

Test Accuracy	10^{-1}	10^{-2}	10^{-3}	10^{-4}	10^{-5}	10^{-6}
Boxline						
Failed points with Dble	0.002‰	0.008‰	0.01‰	0.05 ‰	0.1 ‰	0.4 ‰
Failed pts with LU	none	none	none	none	none	none
Failed points with LU and Gram	none	none	none	none	none	none
Penline						
Failed points with Dble	0.1‰	0.3‰	0.8‰	2 ‰	0.9 %	3.7%
Failed pts with LU	0.002‰	0.008 ‰	0.04‰	0.09 ‰	0.3 ‰	1 ‰
Failed points with LU and Gram	none	none	none	0.002 ‰	0.07 ‰	0.2‰
Hexline						
Failed points with Dble	2‰	5‰	1.1%	2.8 %	7.6 %	18.1 %
Failed pts with LU	0.1‰	0.3 ‰	1‰	5 ‰	1.7 %	5.5%
Failed points with LU and Gram	0.08‰	0.3 ‰	1‰	4 ‰	1.4 %	4.8%

Table 4. Fraction of unstable points, out of the sample of $5 \cdot 10^5$ events, depending on the accuracy of the gauge test for the abelian contributions.

Test Accuracy	10^{-1}	10^{-2}	10^{-3}	10^{-4}	10^{-5}	10^{-6}
BoxlineNoAbe						
Failed points with Dble	0.008‰	0.03‰	0.07‰	0.2 ‰	0.6 ‰	1.8 ‰
Failed pts with LU	none	0.01 ‰	0.04‰	0.1 ‰	0.3 ‰	1‰
Failed points with LU and Gram	none	0.008 ‰	0.03‰	0.08 ‰	0.3 ‰	0.8‰
PenlineNoAbe						
Failed points with Dble	none	0.004‰	0.01‰	0.3 ‰	4.6 %	3.6%
Failed pts with LU	none	0.002 ‰	0.006‰	0.1 ‰	1.3 ‰	1.2%
Failed points with LU and Gram	none	none	0.004‰	0.08 ‰	0.7 ‰	7‰
HexlineNoAbe						
Failed points with Dble	0.5‰	1.2‰	4.1‰	1.4 %	4.4 %	12%
Failed pts with LU	0.03 ‰	0.08‰	0.3‰	1.6 ‰	8 ‰	3.2 %
Failed pts with LU and Gram	0.02 ‰	0.04‰	0.2‰	0.9 ‰	4 ‰	1.9 %

Table 5. Fraction of unstable points, out of the sample of $5 \cdot 10^5$ events, depending on the accuracy of the gauge test for the non-abelian contributions.

which avoids the explicit calculation of inverse Gram determinants of eq. (A.7) by solving numerically a system of linear equations, eq. (A.10). It turns out that this procedure is more stable close to singular regions and reduces considerably the number of identified instabilities without CPU penalty, tables 4 and 5. In addition, we apply also special tensor reduction routines for small Gram determinants in analogy to ref. [70] using eq. (A.11). These routines are switched on whenever a cancellation in the Gram determinant estimated in our set up by the inverse of Δ,

$$\Delta = \frac{2\sum_{i_1\ldots i_n=1}^{n} \epsilon_{i_1\ldots i_n} p_1 \cdot p_{i_1} \ldots p_n \cdot p_{i_n}}{2\sum_{i_1\ldots i_n=1}^{n} |\epsilon_{i_1\ldots i_n} p_1 \cdot p_{i_1} \ldots p_n \cdot p_{i_n}|}, \tag{3.3}$$

JHEP10(2011)070

is larger than a given cut off. The milder the cancellation the larger the number of terms in the expansion that has to be included to provide a good accuracy. For C_{ij} (D_{ij}) functions, we include tensor integrals up to rank 9 (7) which guarantees approximately an error of $\mathcal{O}(\Delta^7)$ ($\mathcal{O}(\Delta^4)$) for the C_{ij} (D_{ij}) tensor coefficients of rank 2 (rank 3).[7] Such that, e.g. the cancellation of two digits in the Gram determinant typically results in a precision of 14 (8) digits for the C_{ij} (D_{ij}) tensor coefficients of rank 2 (rank 3). Cancellations of two to three digits resulting in $\Delta \propto \mathcal{O}(10^{-2,-3})$ in the Gram determinant of the D functions represent the borderline, in our present set up, for which the special tensor reduction routines for D_{ij} functions provide better results than the ones obtained with the LU decomposition. Practically, below the cut off on Δ, we compare the precision provided by the two methods using sum rules and apply the most precise one. In tables 4 and 5, one can see that up to the penline(NoAbe) contribution, the combined method, denoted in the tables by "LU and Gram", works well leaving the remaining instabilities below the per mill level for an accuracy of the gauge test of 10^{-4}. Note, however, that for the boxlineNoAbe and the penlineNoAbe routines the behavior is worse than for the abelian contributions. In these cases, cancellations in the calculation of Cayley determinants in C and/or D functions also take place and other special routines have to be applied, ref. [70].

For the hexagons, the remaining instabilities are still considerable and, generically, cancellations in Cayley determinants of the E and F functions are also present. At this stage, the simplest and fastest way of rescuing the remaining instabilities is calling the contributions with quadruple (QUAD) precision. However, quadruple precision is 20 times slower than double (Dble) precision, thus, revaluating the identified unstable points, 5% of the points for the hexline contribution (the most time consuming and most unstable object) for an accuracy of the Ward identity gauge test of 10^{-6}, results in an addition of 100% CPU time. A better approach which reduces the slowing factor of QUAD precision consists in applying QUAD precision to compute the input scalar and the tensor coefficient integrals. The tensor decomposition routines and scalar integrals amount a fraction of the total CPU time of the hexline(NoAbe) routines and evaluating these in QUAD precision results in routines only a factor 4 slower than the original one. Therefore, for instabilities at the 5% level, only an additional 20% CPU time is added, in contrast to the 100% when applying quadruple precision to the whole routine. After this procedure, the instabilities are reduced for an accuracy of 10^{-6} approximately a 300 factor for the hexagon contributions, leaving the instabilities at the $\approx 0.15‰$ level, confirming that the lost of accuracy is at the level of the tensor integral coefficient determination due to cancellations in the Gram and/or Cayley determinants. For this reduced set of points, $\approx 0.15‰$, table 6, we can call the routines with full QUAD precision ("Full QUAD" in tables) with only an additional 5 ‰ CPU time, reducing the instabilities by an order of magnitude. In tables 6 and 7, the fraction of unstable points after these steps depending on the accuracy demanded for the Ward identity gauge test are shown for the abelian and the non-abelian contributions, respectively, for two setups, with (Set up 1) and without (Set up 2) previously applying

[7] For D functions, cancellations in more than one sub-determinant can appear. Nevertheless, the estimate seems to work.

JHEP10(2011)070

Test Accuracy	10^{-1}	10^{-2}	10^{-3}	10^{-4}	10^{-5}	10^{-6}
Boxline						
Set up 1						
Failed points with LU	none	none	none	none	none	none
Failed pts with QUAD	none	none	none	none	none	none
Failed points with Full QUAD	none	none	none	none	none	none
Set up 2						
Failed points with LU and Gram	none	none	none	none	none	none
Failed pts with QUAD	none	none	none	none	none	none
Failed points with Full QUAD	none	none	none	none	none	none
Penline						
Set up 1						
Failed points with LU	0.002‰	0.008‰	0.04 ‰	0.09‰	0.3‰	0.1 %
Failed pts with QUAD	none	none	none	none	none	0.002‰
Failed pts with full QUAD	none	none	none	none	none	0.002‰
Set up 2						
Failed points with LU and Gram	none	none	none	0.002 ‰	0.07‰	0.2‰
Failed pts with QUAD	none	none	none	none	none	none
Failed points with Full QUAD	none	none	none	none	none	none
Hexline						
Set up 1						
Failed points with LU	0.1‰	0.3‰	1‰	5 ‰	1.6 %	5.5 %
Failed pts with QUAD	none	none	none	none	0.02 ‰	0.19‰
Failed points with Full QUAD	none	none	none	none	0.004 ‰	0.07‰
Set up 2						
Failed points with LU and Gram	0.08‰	0.3‰	1‰	4 ‰	1.4 %	4.8 %
Failed pts with QUAD	none	none	none	none	0.018 ‰	0.15‰
Failed points with Full QUAD	none	none	none	none	0.002 ‰	0.03‰

Table 6. Fraction of unstable points, out of the sample of $5 \cdot 10^5$ events, depending on the accuracy of the gauge test for Dble and QUAD precision for the abelian contributions.

the special routines for small Gram determinants. The non-existence of instabilities for an accuracy of the Ward identity gauge test of 10^{-4}, both for the hexline and for the hexlineNoAbe routines, without using the special routines for small Gram determinants in double precision, suggests that an increase of precision would be enough to rescue these points, and also that the Landau singularities are not present for cut accepted points or they are the sub-million level for the kinematics of EW $pp \to W^+W^-jj + X$ production and given the cuts of eqs. (3.1), (3.2). Once, we are forced to use QUAD precision for the hexagons, the use of the special routines does not bring too much of an improvement concerning the final number of instabilities but it introduces a delaying factor. To reduce this factor, we only switch on the special routines whenever the cancellation of the Gram

JHEP10(2011)070

Test Accuracy	10^{-1}	10^{-2}	10^{-3}	10^{-4}	10^{-5}	10^{-6}
BoxlineNoAbe						
Set up 1						
Failed points with LU	none	0.01‰	0.04‰	0.1 ‰	0.3 ‰	1 ‰
Failed pts with QUAD	none	none	none	none	0.002 ‰	0.01‰
Failed pts with Full QUAD	none	none	none	none	none	0.002‰
Set up 2						
Failed points with LU and Gram	none	0.008‰	0.03‰	0.08 ‰	0.3 ‰	0.8 ‰
Failed pts with QUAD	none	none	none	none	none	0.008‰
Failed points with Full QUAD	none	none	none	none	none	none
PenlineNoAbe						
Set up 1						
Failed points with LU	none	0.002‰	0.006‰	0.1 ‰	1 ‰	1.2%
Failed pts with QUAD	none	none	none	none	none	0.002‰
Failed points with Full QUAD	none	none	none	none	none	0.002‰
Set up 2						
Failed points with LU and Gram	none	none	0.004‰	0.08 ‰	0.7 ‰	0.76%
Failed pts with QUAD	none	none	none	none	none	none
Failed points with Full QUAD	none	none	none	none	none	none
HexlineNoAbe						
Set up 1						
Failed points with LU	0.03‰	0.08‰	0.3‰	1.6 ‰	0.8%	3.3%
Failed pts with QUAD	none	none	none	none	0.05 ‰	0.4 ‰
Failed pts with Full QUAD	none	none	none	none	0.006 ‰	0.008 ‰
Set up 2						
Failed points with LU and Gram	0.02‰	0.04‰	0.2‰	0.9 ‰	0.4%	1.9%
Failed pts with QUAD	none	none	none	none	0.002 ‰	0.15 ‰
Failed pts with Full QUAD	none	none	none	none	none	0.002 ‰

Table 7. Fraction of unstable points, out of the sample of $5 \cdot 10^5$ events, depending on the accuracy of the gauge test for Dble and QUAD precision for the non-abelian contributions.

determinant are severe, larger than 3 digits, $\Delta \lessapprox 10^{-4}$. This procedure is used to compute the timing of the routines in tables 8 and 9. In these tables, one finds the average CPU time for the evaluation of the abelian and non-abelian type contributions, respectively, including a detailed description of how this time is distributed for the calculation of the Ward identity gauge tests, different helicities and the revaluation of unstable points with QUAD precision using a single core of an Intel(R) Core(TM)2 Quad CPU Q6600 @ 2.40GHz computer with the Intel FORTRAN compiler. We observe that most of the time of the hexline(NoAbe) routine is spent in applying the Ward identity gauge tests despite the fact that not all of the routine should be revaluated, table 1. We can reduce this slowing factor without affecting statistically the identified number of instabilities given in tables 6 and 7

JHEP10(2011)070

	boxline	penline	hexline
CPU time	8μ s	70μ s	2 ms
additional CPU time for Gauge Test	8%	30%	28%
n^o Gauge Test	2	3	4
Total additional CPU time for Gauge Test	16%	90 %	112 %
additional CPU time for spinor helicity	12%	5%	1%
n^o Helicity(Worse Case)	2	2	2
Total additional CPU time for Helicity	24%	10%	2%
Average failed Gauge test(Accuracy 10^{-6})	none	0.3‰	5%
Average additional CPU time for bad point QUAD precision	0	4.6‰	20%
Additional CPU time for revaluate gauge tests	0	4.1‰	5.6%
Total CPU time (See test)	11.2μ s	141μ s	4.8(3) ms
Final Instabilities	none	none	0.07‰

Table 8. Average CPU time per point for the abelian contributions including additional time spent performing gauge tests and rescuing unstable points.

	boxlineNoAbe	penlineNoAbe	hexlineNoAbe
CPU time	6μ s	60μ s	2 ms
additional CPU time for Gauge Test	10%	20%	40%
n^o Gauge Test	1	2	3
Total additional CPU time for Gauge Test	10%	40%	120%
additional CPU time for spinor helicity	14%	8.5%	1%
n^o Helicity(Worse Case)	2	2	2
Total additional CPU time for Helicity	28%	19%	2%
Average failed Gauge test(Accuracy 10^{-6})	0.1‰	1.2%	3%
Average additional CPU time for bad point QUAD precision	1.5‰	27%	12%
Additional CPU time for revaluate gauge tests	0.01‰	0.5%	3.6%
Total CPU time (See test)	8μ s	111μ s	4.8(3) ms
Final Instabilities	0.002‰	0.002‰	0.02‰

Table 9. Average CPU time per point for the non-abelian contributions including additional time spent performing gauge tests and rescuing unstable points.

by applying instead of the four (three) gauge tests for the hexline(NoAbe) contributions only one selected randomly. The total CPU time in parenthesis in tables 8 and 9 is computed applying this procedure. Moreover, the time shown is referred to the calculation of the finite pieces $\widetilde{\mathcal{M}}_v$ since we will assume that the divergent pieces and $\widetilde{\mathcal{N}}_v$ for complete processes are known analytically, such that, we do not have to revaluate $\widetilde{\mathcal{M}}_v$ and $\widetilde{\mathcal{N}}_v$ for the divergent part of the input functions.

JHEP10(2011)070

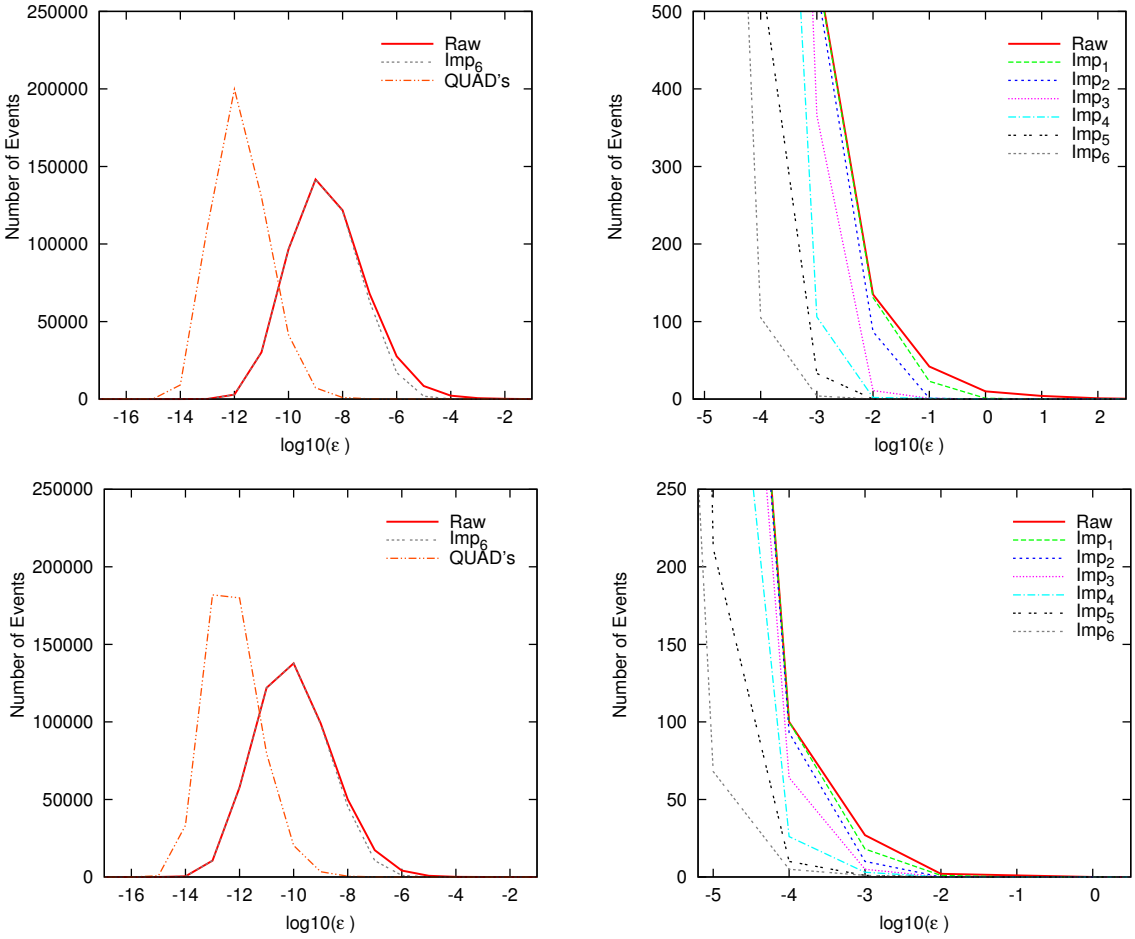

Figure 16. The normalized difference between Double precision and Quadruple precision for the hexline (top) and the hexlineNoAbe (bottom) contributions is represented by the "Raw" line. "QUAD's" represents the difference between the amplitudes evaluated with QUAD precision and with QUAD only applied to the basis of scalar and tensor integral routines. "Imp$_X$" represents the effect of the rescue system activated for an accuracy of the Ward identity gauge test of 10^{-X}. The right panels describe the critical region where double precision is not accurate and the effect of the rescue system for different values of the Ward identity gauge test.

In figure 16, the relative accuracy of the double precision result, ϵ_0, defined as the absolute value of the difference between the double and quadruple precision divided by the quadruple precision result is plotted. We also plot represented by the "QUAD's" label, the difference between the amplitudes evaluated with full QUAD precision and with QUAD only applied to the basis of scalar integrals and tensor integral routines dotted-dashed line. The effect of the rescue system, i.e., the double result is set to the QUAD precision when the Ward identity gauge test for the amplitudes fails at the accuracy $10^{-(X)}$ are described by the "Imp$_X$" lines. In the right panels, one can see the critical region, where double precision is not accurate, and the effect of the rescue system for different values of the Ward identity gauge test. One observes that the choice 10^{-4} (Imp$_4$) gives 3 digits of precision at the per mill level with non-identified left instabilities at this level of accuracy,

JHEP10(2011)070

tables 6 and 7. From the plot, we can conclude that the Ward identity gauge test together with the use of QUAD precision is an efficient system to control the accuracy of our results.

4 Conclusions

In this paper, some of the NLO QCD one-loop amplitudes contributing to the process $pp \to VVjj + X$ have been computed. It has been shown that the numerical instabilities due to the presence of small Gram and Cayley determinants are under control. The use of the LU decomposition method for C and D functions reduces considerably the fraction of unstable points at the double precision level (without CPU penalty). This improvement together with the use of special routines for small Gram determinants is enough to reduce the instabilities for pentagons well bellow the per mill level for an accuracy of the Ward Identity gauge test of 10^{-4}. Using quadruple precision in two steps, the instabilities for the hexagons for a precision of 10^{-6} in the Ward identity gauge tests are reduced up to the 0.03‰ level. To decrease further this number the use of higher precision can be safely applied since for an accuracy of 10^{-4} the identified instabilities disappear even without previously using special routines for small Gram determinants. This suggests that the presence of Landau singularities which translate into exactly vanishing Cayley determinants and the appearance of exactly vanishing Gram determinants are small for the kinematics of EW $pp \to WWjj + X$ production, given the cuts of eqs. (3.1) and (3.2).

It has been shown factorization proofs of the infrared divergences of the bosonic contributions of $VVVV$ and $VVVj$ production with $V \in (W, Z, \gamma)$. We have also given the master equations for the evaluation of the tensor coefficient integrals in the external convention including those needed for small Gram determinants.

The CPU time of the contributions involving hexagons, which rounds the milliseconds, are competitive with other more sophisticated methods. We plan to use these tools not only to compute diboson plus two jet production at hadron colliders at NLO QCD, but also other interesting $2 \to 4$ processes like $W\gamma\gamma + j$ [82].

Acknowledgments

F.C thanks M. Rauch for pointing out the LU method, D. Zeppenfeld for encouraging discussions and S. Khodayar for reading the manuscript. F.C. acknowledges partial support of a postdoctoral fellowship of the Generalitat Valenciana, Spain (Beca Postdoctoral d'Excel·lència), by European FEDER and Spanish MICINN under grant FPA2008-02878 and by the Deutsche Forschungsgemeinschaft via the Sonderforschungsbereich/Transregio SFB/TR-9 "Computational Particle Physics". The Feynman diagrams in this paper were drawn using Axodraw [100].

A Tensor decomposition master equations

For the derivation of the Master Equations presented in this appendix, we have followed closely ref. [70]. The difference resides in the convention used to derive them. Meanwhile ref. [70] uses the internal propagator momenta, q_k, we use the external momenta, p_k. The

JHEP10(2011)070

conversion from one notation to the other is trivial. Nevertheless, we have derived the recursion relations in this notation, first, to avoid loss of accuracy in the conversion for critical points, second, the conversion for pentagons and hexagons of high rank starts to be lengthy and time consuming.

The n-point one loop tensor/scalar integrals can be written as

$$I_N^{\mu_1\dots\mu_P}(p_1,\dots,p_{N-1},m_0,\dots,m_{N-1}) = c_\Gamma(\mu^2)\int d^Dl\frac{l^{\mu_1}\dots l^{\mu_p}}{N_0\dots N_{N-1}}, \qquad P\geq 0 \tag{A.1}$$

with

$$c_\Gamma(\mu^2) = \frac{-i(4\pi)^{D/2}(\mu^2)^{(4-D)/2}}{(2\pi)^D\Gamma(3-D/2)}, \tag{A.2}$$

and

$$N_k = (l+q_k)^2-m_k^2+i\epsilon = \left(l+\sum_{j=0}^{k}p_j\right)^2-m_k^2+i\epsilon, \quad k=0,\dots,N-1, \quad q_0=p_0=0. \tag{A.3}$$

Although the introduction of external momenta may seem an additional complication, if one carelessly uses the internal propagator notation but uses external momenta in their expressions, the number of terms grow factorially. As an example, we present the tensor integral of rank 1 for a box integral. With the external momenta convention, the tensor integral is written in terms of their tensor integral coefficients as,

$$I_4^{\mu_1}(p_1,p_2,p_3) = D_1p_1^{\mu_1}+D_2p_2^{\mu_1}+D_3p_3^{\mu_1}. \tag{A.4}$$

If we use the internal momenta notation, IM, for the same integral and translate it to the external momenta notation to apply equation of motions or transversality properties, the number of terms increases from 3 to 6:

$$\begin{aligned} I_4^{\mu_1}(q_1,q_2,q_3) &= D_1^{IM}q_1+D_2^{IM}q_2+D_3^{IM}q_3 \\ &= D_1^{IM}p_1^{\mu_1}+D_2^{IM}(p_1+p_2)^{\mu_1}+D_3^{IM}(p_1+p_2+p_3)^{\mu_1}. \end{aligned} \tag{A.5}$$

For Hexagons of rank 5, this means passing from 4500 to 200000 terms. Although, this problem can be solved trivially, e.g., applying conservation of momentum, some care has to be taken to avoid exceeding the memory capacities of the computer at intermediate stages.

Generally, the tensor integrals are written in terms of its tensor integral coefficients using Lorentz-covariant structures,

$$I_N^{\mu_1\dots\mu_P} = \sum_{n=0}^{[P/2]}\sum_{i_{2n+1},\dots,i_P=1}^{N-1}\{\underbrace{g\dots g}_{n}p\dots p\}_{i_{2n+1}\dots i_P}^{\mu_1\dots\mu_P}I^N_{\underbrace{0\dots0}_{2n}i_{2n+1}\dots i_P} \tag{A.6}$$

where the curly braces are defined similarly as in ref. [70].

Following ref. [70], we find for the external momenta convention up to the pentagon level, the following Master equations for the tensor coefficient integrals:

$$I^N_{i_1\dots i_P} = \sum_{n=1}^{N-1}(Z^{(N-1)})^{(-1)}_{i_1n}\left(S^{(N-1)}_{ni_2\dots i_P}-2\sum_{r=2}^{P}\delta_{ni_r}I^N_{00i_2\dots\hat{i}_r\dots i_P}\right),$$

$$N\leq 5, \quad 1\leq i_n\leq N-1$$

JHEP10(2011)070

$$I^N_{00i_3\ldots i_P} = \frac{1}{2(D+P-N)}\Bigg((-1)^{(\delta_{0(i_3)_0}+\ldots+\delta_{0(i_P)_0})} I^{(N-1)}_{i3\ldots i_P}(0) + 2m_0^2 I^N_{i_3\ldots i_P} + \sum_{n=1}^{N-1}(r_n - r_{n-1}) I^N_{ni3\ldots i_P}\Bigg), \qquad N \leq 5, i_3 \ldots i_P = 0, \ldots N-1 \tag{A.7}$$

$(Z^{(N-1)})^{(-1)}$ is the inverse Gram determinant which is built with external momenta, $Z_{ij} = 2(p_i \cdot p_j)$ and $r_n = \left(\sum_{j=1}^n p_j\right)^2 - m_n^2$. $S^{N+1}_{ji_2\ldots i_P}$ is defined by

$$S^{N+1}_{ji_2\ldots i_P} = \bar{\delta}_{N(i_2)_j} \ldots \bar{\delta}_{N(i_P)_j} I^N_{(i_2)_j\ldots(i_P)_j}(j) - (-1)^{(\delta_{0(i_2)_{j-1}}+\ldots+\delta_{0(i_P)_{j-1}})} I^N_{(i_2)_{j-1}\ldots(i_P)_{j-1}}(j-1) - (r_j^2 - r_{j-1}^2) I^{N+1}_{i_2\ldots i_p}\,, \tag{A.8}$$

$\bar{\delta}_{ij} = 1 - \delta_{ij}$, $(i_1)_j$ is given by,

$$(i_1)_j = \begin{pmatrix} i_1 \leq j & i_1 \\ i_1 > j & i_1 - 1 \end{pmatrix}, \tag{A.9}$$

and j in $I^{(N)}_{i_1\ldots}(j)$ means that the N_j propagator has been canceled, that is, the tensor coefficients for the tensor integral with the N_j propagator removed from $I^{(N+1)}_{i_1\ldots}$. For the LU implementation, the inversion of the Matrix in eq. (A.7) is not done analytically, instead, a system of equations for the tensor integrals given by,

$$(Z^{(N-1)})_{i_1 n} I^N_{i_1\ldots i_P} = S^{(N-1)}_{ni_2\ldots i_P} - 2\sum_{r=2}^{P} \delta_{ni_r} I^N_{00i_2\ldots\hat{i}_r\ldots i_P}, \tag{A.10}$$

is solved using a fast implementation of partial pivoting of the LU decomposition method. For small Gram determinants, we define in analogy to ref. [70],

$$\begin{aligned} \hat{S}^{N+1}_{ji_2\ldots i_P} &= \bar{\delta}_{N(i_2)_j} \ldots \bar{\delta}_{N(i_P)_j} I^N_{(i_2)_j\ldots(i_P)_j}(j) - (-1)^{(\delta_{0(i_2)_{j-1}}+\ldots+\delta_{0(i_P)_{j-1}})} I^N_{(i_2)_{j-1}\ldots(i_P)_{j-1}}(j-1) \\ S^{N+1}_{00i_3\ldots i_P} &= 2(-1)^{(\delta_{0(i_3)_0}+\ldots+\delta_{0(i_P)_0})} I^N_{(i_3)_0\ldots(i_P)_0}(0) + 2\,m_0^2\, I^{N+1}_{(i_3)_0\ldots(i_P)_0}, \end{aligned} \tag{A.11}$$

and the recursion relations are obtained directly from eqs. (5.41-5.48) of ref. [70] using external momenta in all (sub)determinants and the replacement $f_n \to (r_n - r_{n-1})$. We have implemented these recursion relations up to rank 9 for the C_{ij}, and up to rank 7 for the D_{ij} functions.[8]

For the pentagons, we have followed closely section 6 of ref. [70] and derived their master formulas eqs. (6.12,6.13) for the external momenta convention. Although, the cancellation that takes place to get their simple equations are different, the final master integrals

[8] The UV part of the integrals are not given explicitly here. They can be obtained by contacting the author.

JHEP10(2011)070

are quite similar:

$$
\begin{aligned}
&det(X^{(4)})\bar{E}_{ki_1\ldots i_P} \\
&= \sum_{n=1}^{4} X^{(4)}_{kn}\Big(\bar{\delta}_{i_1 n}\ldots\bar{\delta}_{i_P n} D_{(i_1)_n\ldots(i_P)_n}(n) \\
&\quad -(-1)^{(\delta_{0(i_1)_{j-1}}+\ldots+\delta_{0(i_P)_{j-1}})} D_{(i_1)_{n-1}\ldots(i_P)_{n-1}}(n-1)\Big) \\
&\quad -X^{(4)}_{k0}(-1)^{(\delta_{0(i_1)_0}+\ldots+\delta_{0(i_P)_0})} D_{(i_1)_0-\ldots(i_P)_0}(0) \\
&\quad -2\sum_{n=1}^{4}\sum_{r=1}^{P} X^{4}_{(kn)(0i_r)}\Big((\bar{\delta}_{i_1 n}\ldots\bar{\delta}_{i_{r-1}n}\bar{\delta}_{i_{r+1}n}\ldots\bar{\delta}_{i_P n} D_{00(i_1)_n\ldots\widehat{(i_r)_n}\ldots(i_P)_n}(n) \\
&\quad -(-1)^{(\delta_{0(i_2)_{j-1}}+\ldots+\delta_{0(i_{r-1})_{j-1}}+\delta_{0(i_{r+1})_{j-1}}+\ldots+\delta_{0(i_P)_{j-1}})} D_{00(i_1)_{n-1}\ldots\widehat{(i_r)_{n-1}}\ldots(i_P)_{n-1}}(n-1)\Big) \\
&\qquad\qquad\qquad\qquad k=1,\ldots,4, \qquad\qquad P<4, \qquad\qquad (A.12)
\end{aligned}
$$

$$
\begin{aligned}
&det(X^{(4)})\bar{E}_{00i_2\ldots i_P} \\
&= \sum_{n=1}^{4} X^{(4)}_{n0}\Big(\bar{\delta}_{i_2 n}\ldots\bar{\delta}_{i_P n} D_{00(i_2)_n\ldots(i_P)_n}(n) \\
&\quad -(-1)^{(\delta_{0(i_2)_{j-1}}+\ldots+\delta_{0(i_P)_{j-1}})} D_{00(i_2)_{n-1}\ldots(i_P)_{n-1}}(n-1)\Big), \qquad\qquad P<4, \qquad\qquad (A.13)
\end{aligned}
$$

where $X^{(4)}$ and related quantities are defined/obtained from eq. (2.23) in ref. [70] making the replacement $f_n \to (r_n - r_{n-1})$ and using directly external momenta, $q_k \to p_k$.

For the hexagons, we have followed section 7 of ref. [70]. The master equations with external momenta convention are obtained from their eqs. (7.13,7.16-7.18) by making the replacement:

$$
E_{i_2 i_3\ldots i_P}(0) \to (-1)^{(\delta_{0(i_2)_{n-1}}+\ldots+\delta_{0(i_P)_{n-1}})} E_{(i_2)_{n-1}\ldots(i_P)_{n-1}}(n-1), \qquad (A.14)
$$

using directly external momenta, $q_k \to p_k$. We have checked the derivation of all the tensor coefficients up to Hexagons of rank 5 by contracting the tensor integrals with external momenta. Thus, we can relate all the tensor coefficients of order N and rank P to tensor integrals of order N and $N-1$ and rank $P-1$:

$$
\begin{aligned}
p_{i\mu_1} p_{j\mu_2}\ldots p_{k\mu_P} I_N^{\mu_1\ldots\mu_P} &= \sum_{i_1\ldots i_P}^{N-1} Z_{ii_1} Z_{ji_2}\ldots Z_{ki_P} I^N_{i_1\ldots i_P} \qquad (A.15)\\
&= p_{j\mu_2}\ldots p_{k\mu_P}(I^{\mu_2\ldots\mu_P}_{N-1}(i) - I^{\mu_2\ldots\mu_P}_{N-1}(i-1) - (r_i - r_{i-1}) I^{\mu_2\ldots\mu_P}_N).
\end{aligned}
$$

For hexagons of rank 5, up to 166 different combinations (not all of them independent since only four momenta out of six are linearly independent) where built and checked at the FORTRAN and Mathematica level. The implementation of these routines together with the massless input integrals in Mathematica have proved to be quite useful since we can overcome the loss of accuracy due to small Gram determinants by increasing the

JHEP10(2011)070

working precision, and check accurately the special routines for small Gram determinants, the tensor reductions for pentagons a la Passarino Veltman vs a la Denner-Dittmaier as well as the complete numerical result of the contributions.

B Benchmark numbers for the hexagon contributions

In this section, we provide numbers for the hexline and the hexlineNoAbe contributions. The set of momenta used for $q(p_1)\bar{q}(p_2)V_1V_2V_3g \to 0$ is chosen to be:

$$\begin{aligned}
p_1 &= (2210.591640000411,0,0,2210.591640000411)\,,\\
p_2 &= (410.6465697388802,0,0,-410.6465697388802)\,,\\
p_{V_1} &= (-1644.598252136518,-186.7167811992445,14.28499809343437,-1633.902137026130)\,,\\
p_{V_2} &= (-266.9005208707261,-59.67643702980636,-176.1526035584612,-173.8364669053697)\,,\\
p_{V_3} &= (-402.5905961231937,166.3844370751274,218.6277243718783,-283.2688206929862)\,,\\
p_g &= (-307.1488406088535,80.00878115392345,-56.76011890685155,291.0623543629552)\,,
\end{aligned} \tag{B.1}$$

with the notation $p = (p^0, p^1, p^2, p^3)$ and all the components given in GeV. This represents a cut-accepted point for the EW $qq \to W^+W^-qq$ process with a "mild" behavior, with "mild" meaning that there are not small Gram/Cayley determinants appearing up to the hexagon level, therefore the double precision routines provide accurate results. The corresponding polarization vectors are constructed following the conventions of ref. [99], eq. (A.11). First, we give results for each of the diagrams that constitute the hexline contribution for a particular permutation of the electroweak vector bosons, $\mathcal{M}_{V_1V_2V_3g,\tau}$, with $\tau = -1$, in table 10 and table 11, using the decomposition,

$$\begin{aligned}
2\frac{\mathrm{Re}\left(\mathcal{M}^B_\tau \cdot \mathcal{M}^*_{V_1V_2V_3g,\tau}\right)}{|\mathcal{M}^B_\tau \mathcal{M}^{B*}_\tau|} &= \frac{g_0^2}{(4\pi)^2}(4\pi)^\epsilon\Gamma(1+\epsilon)(\mu_0)^{-2\epsilon}\sum_{n=1}^{13}\left(\frac{\mathcal{C}_n^{V_1V_2V_3g}}{T^a}\right)\\
&\times\left(c^{(n)}_{(0),V_1V_2V_3g}+\frac{c^{(n)}_{(1),V_1V_2V_3g}}{\epsilon}+\frac{c^{(n)}_{(2),V_1V_2V_3g}}{\epsilon^2}+\frac{(D-4)}{-2\epsilon}d^{(n)}_{(0),V_1V_2V_3g}+\frac{(D-4)}{-2\epsilon}\frac{d^{(n)}_{(1),V_1V_2V_3g}}{\epsilon}\right),
\end{aligned} \tag{B.2}$$

correspondingly to eq. (2.21). $\mathcal{M}^B_\tau = \mathcal{M}^B_{V_1V_2V_3g\tau}$, i.e. the born amplitude for the specific order of vector bosons. The $(4\pi)^\epsilon\Gamma(1+\epsilon)(\mu_0)^{-2\epsilon}$ factor comes from the definition for the scalar and tensor integrals, eq. (A.1). We can implement some tests to these numbers. Assuming a general common factor, C_F, we can check the value of the sum of $c^{(n)}_{(0),V_1V_2V_3g}$ by testing the factorized scale energy independence, similarly as eq. (2.41) through,

$$\sum c^{(n)}_{(0),V_1V_2V_3g}(\mu_0) - 2\mathrm{Re}\left(f(s,t,u,\mu_0,1,0,0)^*\right) \not\equiv F(\mu_0) \tag{B.3}$$

with $f(s,u,t,\mu_0,1,0,0)$ given by eq. (2.42) with $s = (p_1+p_2)^2, t = (p_1+p_g)^2$ and $u = (p_2+p_g)^2$. In table 12, we show the values of the sum of $c^{(n)}_{(0),V_1V_2V_3g}$ and $f(s,u,t,\mu_0,1,0,0)$ for two different sets of factorization energy scales, for $\mu_0 = s$, corresponding to the values given in table 10, and for $\mu_0 = 1$GeV. One can see that eq. (B.3) is satisfied with an

JHEP10(2011)070

	$c^{(n)}_{(0),V_1V_2V_3g}$	$c^{(n)}_{(1),V_1V_2V_3g}$	$c^{(n)}_{(2),V_1V_2V_3g}$
n=1	-0.8495224242548815E+02	-0.2718191945175511E+02	-0.3999999999999874E+01
n=2	0.7373715226545116E+02	0.1475364608414150E+02	-0.4823858365463354E-13
n=3	0.7720679379271682E+02	0.1032635756877249E+02	0.4778146726503880E-13
n=4	-0.7023321057368833E+01	-0.2247107183707837E+01	-0.2411275830791782E-14
n=5	0.5075981735087911E+01	0.0000000000000000E+00	0.0000000000000000E+00
n=6	-0.1241513230258542E+03	-0.1483523289520358E+02	0.3441661498683095E-13
n=7	0.1268199899143818E+02	0.2000000000000156E+01	0.1502284155171117E-26
n=8	0.9572211011177236E+01	0.2000000000000001E+01	0.0000000000000000E+00
n=9	0.2215410796479108E+02	0.2000000000000001E+01	0.0000000000000000E+00
n=10	0.1060058346584089E+03	0.1318425587774655E+02	-0.1013265897019504E-13
n=11	-0.1268199899143716E+02	-0.2000000000000000E+01	0.0000000000000000E+00
n=12	-0.1024742028732465E+02	-0.2000000000000000E+01	0.0000000000000000E+00
n=13	-0.1523236618746480E+02	-0.2000000000000000E+01	0.0000000000000000E+00

Table 10. Contributions of the hexline diagrams. $c^{(n)}_{(j),V_1V_2V_3g}$ are defined in eq. (B.2).

	$d^{(n)}_{(0),V_1V_2V_3g,\tau}$	$d^{1,(n)}_{(1),V_1V_2V_3g,\tau}$
n=1	0.8702382558218599E-12	-0.8613060482805703E-13
n=2	0.1709040047358825E-13	-0.8545281855364259E-15
n=3	0.3736943504519546E-13	-0.4397635645750366E-14
n=4	-0.2396002150441086E-13	0.1363187596482680E-15
n=5	0.0000000000000000E+00	0.0000000000000000E+00
n=6	-0.3591236576358064E-12	-0.4690957329075479E-14
n=7	-0.2000000000000079E+01	0.0000000000000000E+00
n=8	-0.2000000000000001E+01	0.0000000000000000E+00
n=9	-0.2000000000000001E+01	0.0000000000000000E+00
n=10	-0.2000000000000000E+01	-0.6325727406404221E-14
n=11	0.2000000000000001E+01	0.0000000000000000E+00
n=12	0.2000000000000001E+01	0.0000000000000000E+00
n=13	0.2000000000000001E+01	0.0000000000000000E+00

Table 11. Contributions of the hexline diagrams. $d^{(n)}_{(j),V_1V_2V_3g}$ are defined in eq. (B.2).

accuracy of 12 digits. Additionally, for this specific phase space point, the Ward identities of eq. (2.26) for the complete contributions are satisfied at the 12 digit level. For the divergent contributions and the rational terms, the factorization against the born amplitude is shown in table 13 through,

$$\sum c^{(n)}_{(1),V_1V_2V_3g} = -6\,, \qquad \sum c^{(n)}_{(1),V_1V_2V_3g} = -4 \quad , \tag{B.4}$$

$$\sum d^{(n)}_{(0),V_1V_2V_3g} = -2\,, \qquad \sum d^{(n)}_{(1),V_1V_2V_3g} = 0, \tag{B.5}$$

JHEP10(2011)070

	$\mu_0 = s$	$\mu_0 = 1\text{GeV}$
$\sum c^{(n)}_{(0),V_1V_2V_3g}$	0.5214540844413348E+02	-0.3135489678574997E+03
$2\text{Re}(f(s,t,u,\mu_0,1,0,0)^*)$	0.1973920880217872E+02	-0.3459551674994638E+03
eq. (B.3)	0.3240619964195476E+02	0.3240619964196406E+02
ratio-1	-0.2868816295631405E-12	

Table 12. Check of factorization scale energy independence through eq. (B.3) for two different sets of factorization energy scales.

	$c^{(n)}_{(1),V_1V_2V_3g}$	$c^{(n)}_{(2),V_1V_2V_3g}$	$d^{(n)}_{(0),V_1V_2V_3g}$
$\sum$	-0.6000000000005826E+01	-0.3999999999999853E+01	-0.1999999999999537E+01
Exact	-0.6000000000000000E+01	-0.4000000000000000E+01	-0.2000000000000000E+01
ratio-1	0.9710010573371619E-12	-0.3674838211509268E-13	-0.4524345419647128E-12

Table 13. Factorization of the divergent contributions through eq. (B.5) against the born amplitude and accuracy.

	$c^{g,(n)}_{(0),V_1V_2V_3}$	$c^{g,(n)}_{(1),V_1V_2V_3}$	$c^{g,(n)}_{(2),V_1V_2V_3}$
n=1	-0.3970812374704999E+02	-0.1265721313949629E+02	-0.1813569591709497E+01
n=2	-0.1350281050903405E+01	-0.7519564890398996E+00	-0.2022904490007958E+00
n=3	0.2728377087017317E+02	0.2055535050768235E+01	-0.5549746075488889E+00
n=4	-0.3264136921557698E+00	-0.1238348703073990E+00	-0.1416214405745540E-01
n=5	0.1723360559577099E+01	0.3328092079219656E+00	0.0000000000000000E+00
n=6	-0.5023976788785847E+02	-0.1779284983273073E+02	-0.2954984559380555E+01
n=7	0.1253736490780382E-02	-0.2491704328619187E-03	-0.7861847392712649E-03
n=8	0.4621898462078639E+00	0.1193463736617884E+00	0.0000000000000000E+00
n=9	0.1418038518281030E+01	0.4012945693937532E+00	0.0000000000000000E+00
n=10	0.1937597641023809E+02	0.8653232589507967E+01	0.1540767536436781E+01

Table 14. Contributions of the hexlineNoAbe diagrams. $c^{g,(n)}_{(j),V_1V_2V_3}$ are defined in eq. (B.6).

correspondingly to eq. (2.44). Note that the numerical values for $d^{(n)}_{(1),V_1V_2V_3g}$ in table 11 are below $10^{(-13)}$.

In the following, we give results for the hexlineNoAbe contribution for $\tau = -1$. We follow the decomposition of eq. (B.6) assuming EW production with an additional jet, thus, the color factor is C_A for all the diagrams,

$$2\frac{\text{Re}\left(\mathcal{M}^B_\tau \cdot \mathcal{M}^{g*}_{V_1V_2V_3,\tau}\right)}{|\mathcal{M}^B_\tau \mathcal{M}^{B*}_\tau|} = \frac{g_0^2}{(4\pi)^2}(4\pi)^\epsilon\Gamma(1+\epsilon)(\mu_0)^{-2\epsilon}\sum_{n=1}^{10} C_A \tag{B.6}$$
$$\times\left(c^{g,(n)}_{(0),V_1V_2V_3} + \frac{c^{g,(n)}_{(1),V_1V_2V_3}}{\epsilon} + \frac{c^{g,(n)}_{(2),V_1V_2V_3}}{\epsilon^2} + \frac{(D-4)}{-2\epsilon}d^{g,(n)}_{(0),V_1V_2V_3} + \frac{(D-4)}{-2\epsilon}\frac{d^{g,(n)}_{(1),V_1V_2V_3}}{\epsilon}\right)$$

JHEP10(2011)070

	$d^{g,(n)}_{(0),V_1V_2V_3}$	$d^{g,(n)}_{(1),V_1V_2V_3}$
n=1	-0.1436483954568111E-11	0.3386511581831592E-13
n=2	-0.6922590837003719E-18	0.1939122411552382E-16
n=3	0.5899544848540121E-13	0.1263944582753722E-13
n=4	-0.5274108820645013E-16	-0.1071274072706729E-17
n=5	0.3633510145273396E-19	0.0000000000000000E+00
n=6	0.5975463630574398E-13	0.1078373100666381E-14
n=7	-0.7861847392712663E-03	0.0000000000000000E+00
n=8	-0.1416214405745516E-01	0.0000000000000000E+00
n=9	-0.1371873399923628E+00	0.0000000000000000E+00
n=10	-0.8478643312109194E+00	0.1159003560547673E-14

Table 15. Contributions of the hexlineNoAbe diagrams. $d^{(n)}_{(j),V_1V_2V_3g}$ are defined in eq. (B.6).

correspondingly to eq. (2.37), with,

$$\mathcal{M}^B_\tau = \mathcal{M}^B_{V_1V_2V_3g,\tau} + \mathcal{M}^B_{V_1V_2gV_3,\tau} + \mathcal{M}^B_{V_1gV_2V_3,\tau} + \mathcal{M}^B_{gV_1,V_2V_3,\tau}, \tag{B.7}$$

that is, the sum of the four Born amplitudes for a given order of the EW vector bosons. The individual contributions are given in table 14 and table 15. In addition, in table 16 we show the hexline results for the four contributions that are mixed under the QCD group for a given permutation of EW vector bosons since they will help us to construct useful checks for the hexlineNoAbe contributions. We use the notation of eq. (B.2) with $\mathcal{M}^B_\tau$ given by eq. (B.7) and provide separate numbers for the sum of the two different color structures that appear in this case. We can check the finite pieces, $c^{(n)}_{(0)}$, by testing the factorized energy scale, μ_0, independence for the two color factors, C_F and C_A through,

- C_F

$$\begin{aligned} &c'_{(0),V_1V_2V_3g}(\mu_0) + c'_{(0),V_1V_2gV_3}(\mu_0) + c'_{(0),V_1gV_2V_3g}(\mu_0) \\ &\quad + c'_{(0),gV_1V_2V_3g}(\mu_0)) - 2\mathrm{Re}\left(f(s,t,u,\mu_0,1,0,0)^*\right) \equiv F(\mu_0) \end{aligned} \tag{B.8}$$

- C_A

$$\begin{aligned} &\frac{-1}{2}\left(c_{(0),V_1V_2V_3g} + c_{(0),V_1V_2gV_3} + c_{(0),V_1gV_2V_3} + c_{(0),gV_1V_2V_3}\right) \\ &\quad + \sum_{j=1}^{10} c^{g,(j)}_{(0),V_1V_2V_3} - 2\mathrm{Re}\left(f(s,t,u,\mu_0,0,1,0)^*\right) \equiv F(\mu_0) \end{aligned} \tag{B.9}$$

similarly to eq. (2.41). The prime quantities are built by adding the two numbers of each line in table 16. For eq. (B.9), $c_{(0)}$ is obtained by taking the number of the second column of each line in table 16. We give the results for two different sets of factorization scale energies in table 17 and the accuracy of it. We obtain 11 digits of precision for the specific

JHEP10(2011)070

	C_F	$C_F - 1/2C_A$
$c_{(0),gV_1V_2V_3}$	0.1186972860337361E+00	-0.2513048326546336E+00
$c_{(0),V_1gV_2V_3}$	-0.3260632362384948E+00	0.1175575424874967E+01
$c_{(0),V_1V_2gV_3}$	-0.3587963452897030E+01	0.6010092883764584E+01
$c_{(0),V_1V_2V_3g}$	0.6748418542481737E+02	-0.2188150305629134E+02
$c_{(1),gV_1V_2V_3}$	0.3435253401752263E-01	-0.2242562120604109E-01
$c_{(1),V_1gV_2V_3}$	-0.1745714679327207E+00	0.9440497420994520E-01
$c_{(1),V_1V_2gV_3}$	-0.9768988228536071E+00	-0.1710884136252724E+00
$c_{(1),V_1V_2V_3g}$	0.1091241185529769E+02	-0.1569618503789184E+02
$c_{(2),gV_1V_2V_3}$	0.0000000000000000E+00	-0.3144738956157922E-02
$c_{(2),V_1gV_2V_3}$	0.0000000000000000E+00	-0.5664857622981814E-01
$c_{(2),V_1V_2gV_3}$	0.6661338147750939E-15	-0.5487493599694454E+00
$c_{(2),V_1V_2V_3g}$	-0.4263256414560601E-13	-0.3391457324843469E+01
$d_{(0),gV_1V_2V_3}$	-0.2765908162227770E-14	0.7861847503483757E-03
$d_{(0),V_1gV_2V_3}$	0.4302114220422482E-15	0.1416214405720360E-01
$d_{(0),V_1V_2gV_3}$	0.4385380947269368E-14	0.1371873399918132E+00
$d_{(0),V_1V_2V_3g}$	0.3652633751016765E-13	0.8478643312106809E+00

Table 16. Contributions of the hexline diagrams for the different colors and for the four permutations for a fixed order of the EW vector bosons.

phase space point. Finally, proceeding in a similar manner from eqs. (2.43), (2.44), the factorization of the divergence contributions can be checked for the two color factors, the results are shown in table 18. The value for all of the $d_{(1)}$ quantities is always below 10^{-13} (not shown). "Exact" for $c_{(1)}$ is given by the 16 first digits of (See eqs. (2.43), (B.2), (B.6)):

$$2 \cdot \mathrm{Re}\left[\left(-\log\left(\frac{-s}{\mu^2}\right)+\log\left(\frac{-t}{\mu^2}\right)+\log\left(\frac{-u}{\mu^2}\right)\right)^*\right]. \tag{B.10}$$

C Color factors

The color factors for the two permutations of the boxline for one gluon emission are given by:

$$\mathcal{C}^{gV}_{(1)} = \mathcal{C}^{Vg}_{(1)} = \mathcal{C}^{gV}_{(2)} = \mathcal{C}^{Vg}_{(3)} = T^a(C_F - 1/2C_A)$$

JHEP10(2011)070

	$\mu_0 = s$	$\mu_0 = 1$
	C_F color factor	
First line of in eq. (B.8)	0.4874171644140917E+02	-0.3169526598603159E+03
$2\mathrm{Re}(f(s,t,u,\mu_0,1,0,0)^*)$	0.1973920880217872E+02	-0.3459551674994638E+03
eq. (B.8)	0.2900250763923045E+02	0.2900250763914789E+02
ratio-1	0.2846611835138901E-11	
	C_A color factor	
First line of eq. (B.9)	-0.4135999643699960E+02	-0.1991502907112327E+03
$2\mathrm{Re}(f(s,t,u,\mu_0,0,1,0)^*)$	0.7711028150622136E+02	0.1260325556690930E+03
eq. (B.9)	0.4322385485937497E+02	0.4322385485945347E+02
ratio-1	-0.1816102823681831E-11	

Table 17. Check of factorization scale energy independence through eqs. (B.8), (B.9) for two different sets of factorization energy scales.

	$c_{(1)}$	$c_{(2)}$	$d_{(0)}$
	C_F color factor		
$\sum$	-5.99999999998432	-3.99999999999893	-1.00000000001008
Exact	-6.00000000000000	-4.00000000000000	-1.00000000000000
ratio-1	-2.612909888455306E-012	-2.668976151198876E-013	1.008459982188015E-011
	C_A color factor		
$\sum$	-11.8662386614969	-2.00000000000024	$<$ E-13
"Exact"	-11.8662386614914	-2.00000000000000	0
ratio-1	4.600764214046649E-013	1.187938636348917E-013	

Table 18. Factorization of the divergent contributions against the born amplitude and accuracy for the two color factors.

$$\mathcal{C}^{Vg}_{(2)} = \mathcal{C}^{gV}_{(3)} = \mathcal{C}^{gV}_{(4)} = \mathcal{C}^{Vg}_{(4)} = T^a C_F. \tag{C.1}$$

The color factors for the penline routines for one gluon emission are given by:

- (gV_1V_2)

$$\begin{aligned} &\mathcal{C}^{gV_1V_2}_{(1)} = \mathcal{C}^{gV_1V_2}_{(2)} = \mathcal{C}^{gV_1V_2}_{(4)} = T^a(C_F - 1/2C_A), \\ &\mathcal{C}^{gV_1V_2}_{(3)} = \mathcal{C}^{gV_1V_2}_{(5)} = \mathcal{C}^{gV_1V_2}_{(6)} = \mathcal{C}^{gV_1V_2}_{(7)} = \mathcal{C}^{gV_1V_2}_{(8)} = T^a C_F, \end{aligned} \tag{C.2}$$

- (V_1gV_2)

$$\begin{aligned} &\mathcal{C}^{V_1gV_2}_{(1)} = \mathcal{C}^{V_1gV_2}_{(2)} = \mathcal{C}^{V_1gV_2}_{(3)} = \mathcal{C}^{V_1gV_2}_{(5)} = T^a(C_F - 1/2C_A), \\ &\mathcal{C}^{V_1gV_2}_{(4)} = \mathcal{C}^{V_1gV_2}_{(6)} = \mathcal{C}^{V_1gV_2}_{(7)} = \mathcal{C}^{V_1gV_2}_{(8)} = T^a C_F, \end{aligned} \tag{C.3}$$

JHEP10(2011)070

- (V_1V_2g)

$$\begin{aligned}\mathcal{C}^{V_1V_2g}_{(1)} &= \mathcal{C}^{V_1V_2g}_{(3)} = \mathcal{C}^{V_1V_2g}_{(6)} = T^a(C_F - 1/2C_A),\\ \mathcal{C}^{V_1V_2g}_{(2)} &= \mathcal{C}^{V_1V_2g}_{(4)} = \mathcal{C}^{V_1V_2g}_{(5)} = \mathcal{C}^{V_1V_2g}_{(7)} = \mathcal{C}^{V_1V_2g}_{(8)} = T^aC_F,\end{aligned} \tag{C.4}$$

the same color factors are obtained for the permutations corresponding to $V_1 \leftrightarrow V_2$ with $V_i \in$ (W$^\pm$,Z,γ).

Finally, the color factors for the one gluon emission case for the hexline routine are given by:

- $(gV_1V_2V_3)$

$$\begin{aligned}\mathcal{C}^{gV_1V_2V_3}_{(1-2)} &= \mathcal{C}^{gV_1V_2V_3}_{(4)} = \mathcal{C}^{gV_1V_2V_3}_{(7)} = T^a(C_F - 1/2C_A)\\ \mathcal{C}^{gV_1V_2V_3}_{(3)} &= \mathcal{C}^{gV_1V_2V_3}_{(5-6)} = \mathcal{C}^{gV_1V_2V_3}_{(8-13)} = T^aC_F\end{aligned} \tag{C.5}$$

- $(V_1gV_2V_3)$

$$\begin{aligned}\mathcal{C}^{V_1gV_2V_3}_{(1-5)} &= \mathcal{C}^{V_1gV_2V_3}_{(8)} = T^a(C_F - 1/2C_A)\\ \mathcal{C}^{V_1gV_2V_3}_{(6-7)} &= \mathcal{C}^{V_1gV_2V_3}_{(9-13)} = T^aC_F\end{aligned} \tag{C.6}$$

- $(V_1V_2gV_3)$

$$\begin{aligned}\mathcal{C}^{V_1V_2gV_3}_{(1-3)} &= \mathcal{C}^{V_1V_2gV_3}_{(5-6)} = \mathcal{C}^{V_1V_2gV_3}_{(9)} = T^a(C_F - 1/2C_A)\\ \mathcal{C}^{V_1V_2gV_3}_{(4)} &= \mathcal{C}^{V_1V_2gV_3}_{(7-8)} = \mathcal{C}^{V_1V_2gV_3}_{(10-13)} = T^aC_F\end{aligned} \tag{C.7}$$

- $(V_1V_2V_3g)$

$$\begin{aligned}\mathcal{C}^{V_1V_2V_3g}_{(1)} &= \mathcal{C}^{V_1V_2V_3g}_{(3)} = \mathcal{C}^{V_1V_2V_3g}_{(6)} = \mathcal{C}^{V_1V_2V_3g}_{(10)} = T^a(C_F - 1/2C_A)\\ \mathcal{C}^{V_1V_2V_3g}_{(2)} &= \mathcal{C}^{V_1V_2V_3g}_{(4-5)} = \mathcal{C}^{V_1V_2V_3g}_{(7-9)} = \mathcal{C}^{V_1V_2V_3g}_{(11-13)} = T^aC_F,\end{aligned} \tag{C.8}$$

the same color factors are obtained for the six other permutations of the vector bosons V_1, V_2 and V_3 with $V_i \in (\mathrm{W}^\pm, Z, \gamma)$.

References

[1] J.M. Campbell, J. Huston and W. Stirling, *Hard interactions of quarks and gluons: a primer for LHC physics*, *Rept. Prog. Phys.* **70** (2007) 89 [hep-ph/0611148] [INSPIRE].

[2] J. Ohnemus, *An order α_s calculation of hadronic W^-W^+ production*, *Phys. Rev.* **D 44** (1991) 1403 [INSPIRE].

[3] L.J. Dixon, Z. Kunszt and A. Signer, *Helicity amplitudes for $O(\alpha_s)$ production of W^+W^-, $W^\pm Z$, ZZ, $W^\pm\gamma$, or $Z\gamma$ pairs at hadron colliders*, *Nucl. Phys.* **B 531** (1998) 3 [hep-ph/9803250] [INSPIRE].

JHEP10(2011)070

[4] L.J. Dixon, Z. Kunszt and A. Signer, *Vector boson pair production in hadronic collisions at order α_s: lepton correlations and anomalous couplings*, *Phys. Rev.* **D 60** (1999) 114037 [hep-ph/9907305] [INSPIRE].

[5] J. Ohnemus, *An order α_s calculation of hadronic $W^{\pm}Z$ production*, *Phys. Rev.* **D 44** (1991) 3477 [INSPIRE].

[6] J. Ohnemus, *Hadronic ZZ, W^-W^+ and $W^{\pm}Z$ production with QCD corrections and leptonic decays*, *Phys. Rev.* **D 50** (1994) 1931 [hep-ph/9403331] [INSPIRE].

[7] U. Baur, T. Han and J. Ohnemus, *WZ production at hadron colliders: effects of nonstandard WWZ couplings and QCD corrections*, *Phys. Rev.* **D 51** (1995) 3381 [hep-ph/9410266] [INSPIRE].

[8] U. Baur, T. Han and J. Ohnemus, *QCD corrections and nonstandard three vector boson couplings in W^+W^- production at hadron colliders*, *Phys. Rev.* **D 53** (1996) 1098 [hep-ph/9507336] [INSPIRE].

[9] J.M. Campbell and R. Ellis, *An update on vector boson pair production at hadron colliders*, *Phys. Rev.* **D 60** (1999) 113006 [hep-ph/9905386] [INSPIRE].

[10] S. Dittmaier, S. Kallweit and P. Uwer, *NLO QCD corrections to WW + jet production at hadron colliders*, *Phys. Rev. Lett.* **100** (2008) 062003 [arXiv:0710.1577] [INSPIRE].

[11] J.M. Campbell, R. Ellis and G. Zanderighi, *Next-to-leading order predictions for $WW + 1$ jet distributions at the LHC*, *JHEP* **12** (2007) 056 [arXiv:0710.1832] [INSPIRE].

[12] F. Campanario, C. Englert, M. Spannowsky and D. Zeppenfeld, *NLO-QCD corrections to $W\gamma j$ production*, *Europhys. Lett.* **88** (2009) 11001 [arXiv:0908.1638] [INSPIRE].

[13] S. Dittmaier, S. Kallweit and P. Uwer, *NLO QCD corrections to $pp/p\bar{p} \to WW$ + jet + X including leptonic W-boson decays*, *Nucl. Phys.* **B 826** (2010) 18 [arXiv:0908.4124] [INSPIRE].

[14] T. Binoth, T. Gleisberg, S. Karg, N. Kauer and G. Sanguinetti, *NLO QCD corrections to ZZ + jet production at hadron colliders*, *Phys. Lett.* **B 683** (2010) 154 [arXiv:0911.3181] [INSPIRE].

[15] F. Campanario, C. Englert, S. Kallweit, M. Spannowsky and D. Zeppenfeld, *NLO QCD corrections to WZ + jet production with leptonic decays*, *JHEP* **07** (2010) 076 [arXiv:1006.0390] [INSPIRE].

[16] F. Campanario, C. Englert and M. Spannowsky, *Precise predictions for (non-standard) $W\gamma$ + jet production*, *Phys. Rev.* **D 83** (2011) 074009 [arXiv:1010.1291] [INSPIRE].

[17] C. Oleari and D. Zeppenfeld, *QCD corrections to electroweak $\nu(l)jj$ and $\ell^+\ell^-jj$ production*, *Phys. Rev.* **D 69** (2004) 093004 [hep-ph/0310156] [INSPIRE].

[18] B. Jager, C. Oleari and D. Zeppenfeld, *Next-to-leading order QCD corrections to W^+W^- production via vector-boson fusion*, *JHEP* **07** (2006) 015 [hep-ph/0603177] [INSPIRE].

[19] G. Bozzi, B. Jager, C. Oleari and D. Zeppenfeld, *Next-to-leading order QCD corrections to W^+Z and W^-Z production via vector-boson fusion*, *Phys. Rev.* **D 75** (2007) 073004 [hep-ph/0701105] [INSPIRE].

[20] T. Melia, K. Melnikov, R. Rontsch and G. Zanderighi, *Next-to-leading order QCD predictions for W^+W^+jj production at the LHC*, *JHEP* **12** (2010) 053 [arXiv:1007.5313] [INSPIRE].

JHEP10(2011)070

[21] T. Melia, K. Melnikov, R. Rontsch and G. Zanderighi, *NLO QCD corrections for W^+W^- pair production in association with two jets at hadron colliders*, *Phys. Rev.* **D 83** (2011) 114043 [arXiv:1104.2327] [INSPIRE].

[22] A. Denner, S. Dittmaier, S. Kallweit and S. Pozzorini, *NLO QCD corrections to $WWbb$ production at hadron colliders*, *Phys. Rev. Lett.* **106** (2011) 052001 [arXiv:1012.3975] [INSPIRE].

[23] G. Bevilacqua, M. Czakon, A. van Hameren, C.G. Papadopoulos and M. Worek, *Complete off-shell effects in top quark pair hadroproduction with leptonic decay at next-to-leading order*, *JHEP* **02** (2011) 083 [arXiv:1012.4230] [INSPIRE].

[24] Z. Bern and D.A. Kosower, *Efficient calculation of one loop QCD amplitudes*, *Phys. Rev. Lett.* **66** (1991) 1669 [INSPIRE].

[25] Z. Bern, L.J. Dixon and D.A. Kosower, *One loop corrections to five gluon amplitudes*, *Phys. Rev. Lett.* **70** (1993) 2677 [hep-ph/9302280] [INSPIRE].

[26] Z. Bern, L.J. Dixon, D.C. Dunbar and D.A. Kosower, *One loop n point gauge theory amplitudes, unitarity and collinear limits*, *Nucl. Phys.* **B 425** (1994) 217 [hep-ph/9403226] [INSPIRE].

[27] Z. Bern, L.J. Dixon, D.C. Dunbar and D.A. Kosower, *Fusing gauge theory tree amplitudes into loop amplitudes*, *Nucl. Phys.* **B 435** (1995) 59 [hep-ph/9409265] [INSPIRE].

[28] Z. Bern, L.J. Dixon and D.A. Kosower, *One loop corrections to two quark three gluon amplitudes*, *Nucl. Phys.* **B 437** (1995) 259 [hep-ph/9409393] [INSPIRE].

[29] Z. Bern, L.J. Dixon and D.A. Kosower, *One loop amplitudes for e^+e^- to four partons*, *Nucl. Phys.* **B 513** (1998) 3 [hep-ph/9708239] [INSPIRE].

[30] R. Britto, F. Cachazo and B. Feng, *Generalized unitarity and one-loop amplitudes in $N = 4$ super-Yang-Mills*, *Nucl. Phys.* **B 725** (2005) 275 [hep-th/0412103] [INSPIRE].

[31] Z. Bern, L.J. Dixon and D.A. Kosower, *On-shell recurrence relations for one-loop QCD amplitudes*, *Phys. Rev.* **D 71** (2005) 105013 [hep-th/0501240] [INSPIRE].

[32] D. Forde and D.A. Kosower, *All-multiplicity one-loop corrections to MHV amplitudes in QCD*, *Phys. Rev.* **D 73** (2006) 061701 [hep-ph/0509358] [INSPIRE].

[33] C.F. Berger, Z. Bern, L.J. Dixon, D. Forde and D.A. Kosower, *Bootstrapping one-loop QCD amplitudes with general helicities*, *Phys. Rev.* **D 74** (2006) 036009 [hep-ph/0604195] [INSPIRE].

[34] G. Ossola, C.G. Papadopoulos and R. Pittau, *Reducing full one-loop amplitudes to scalar integrals at the integrand level*, *Nucl. Phys.* **B 763** (2007) 147 [hep-ph/0609007] [INSPIRE].

[35] C. Anastasiou, R. Britto, B. Feng, Z. Kunszt and P. Mastrolia, *Unitarity cuts and reduction to master integrals in d dimensions for one-loop amplitudes*, *JHEP* **03** (2007) 111 [hep-ph/0612277] [INSPIRE].

[36] G. Ossola, C.G. Papadopoulos and R. Pittau, *Numerical evaluation of six-photon amplitudes*, *JHEP* **07** (2007) 085 [arXiv:0704.1271] [INSPIRE].

[37] S. Badger, E. Glover and K. Risager, *One-loop ϕ-MHV amplitudes using the unitarity bootstrap*, *JHEP* **07** (2007) 066 [arXiv:0704.3914] [INSPIRE].

[38] G. Ossola, C.G. Papadopoulos and R. Pittau, *On the rational terms of the one-loop amplitudes*, *JHEP* **05** (2008) 004 [arXiv:0802.1876] [INSPIRE].

JHEP10(2011)070

[39] R. Ellis, W. Giele and Z. Kunszt, *A numerical unitarity formalism for evaluating one-loop amplitudes*, *JHEP* **03** (2008) 003 [arXiv:0708.2398] [INSPIRE].

[40] G. Ossola, C.G. Papadopoulos and R. Pittau, *CutTools: a program implementing the OPP reduction method to compute one-loop amplitudes*, *JHEP* **03** (2008) 042 [arXiv:0711.3596] [INSPIRE].

[41] W.T. Giele, Z. Kunszt and K. Melnikov, *Full one-loop amplitudes from tree amplitudes*, *JHEP* **04** (2008) 049 [arXiv:0801.2237] [INSPIRE].

[42] P. Mastrolia, G. Ossola, C. Papadopoulos and R. Pittau, *Optimizing the reduction of one-loop amplitudes*, *JHEP* **06** (2008) 030 [arXiv:0803.3964] [INSPIRE].

[43] C. Berger et al., *An automated implementation of on-shell methods for one-loop amplitudes*, *Phys. Rev.* **D 78** (2008) 036003 [arXiv:0803.4180] [INSPIRE].

[44] W. Giele and G. Zanderighi, *On the numerical evaluation of one-loop amplitudes: the gluonic case*, *JHEP* **06** (2008) 038 [arXiv:0805.2152] [INSPIRE].

[45] R. Ellis, W. Giele, Z. Kunszt, K. Melnikov and G. Zanderighi, *One-loop amplitudes for $W+3$ jet production in hadron collisions*, *JHEP* **01** (2009) 012 [arXiv:0810.2762] [INSPIRE].

[46] E. Nigel Glover and C. Williams, *One-loop gluonic amplitudes from single unitarity cuts*, *JHEP* **12** (2008) 067 [arXiv:0810.2964] [INSPIRE].

[47] R. Britto, *Unitarity cuts for one-loop amplitudes*, *Nucl. Phys. Proc. Suppl.* **183** (2008) 36 [INSPIRE].

[48] A. Lazopoulos, *Multi-gluon one-loop amplitudes numerically*, arXiv:0812.2998 [INSPIRE].

[49] Z. Nagy and D.E. Soper, *Numerical integration of one-loop Feynman diagrams for N-photon amplitudes*, *Phys. Rev.* **D 74** (2006) 093006 [hep-ph/0610028] [INSPIRE].

[50] R. Britto and B. Feng, *Integral coefficients for one-loop amplitudes*, *JHEP* **02** (2008) 095 [arXiv:0711.4284] [INSPIRE].

[51] M. Moretti, F. Piccinini and A. Polosa, *A fully numerical approach to one-loop amplitudes*, arXiv:0802.4171 [INSPIRE].

[52] R. Britto, B. Feng and P. Mastrolia, *Closed-form decomposition of one-loop massive amplitudes*, *Phys. Rev.* **D 78** (2008) 025031 [arXiv:0803.1989] [INSPIRE].

[53] R. Britto, B. Feng and G. Yang, *Polynomial structures in one-loop amplitudes*, *JHEP* **09** (2008) 089 [arXiv:0803.3147] [INSPIRE].

[54] A. van Hameren, C. Papadopoulos and R. Pittau, *Automated one-loop calculations: a proof of concept*, *JHEP* **09** (2009) 106 [arXiv:0903.4665] [INSPIRE].

[55] G. Passarino and M. Veltman, *One loop corrections for e^+e^- annihilation into $\mu^+\mu^-$ in the Weinberg model*, *Nucl. Phys.* **B 160** (1979) 151 [INSPIRE].

[56] G. van Oldenborgh and J. Vermaseren, *New algorithms for one loop integrals*, *Z. Phys.* **C 46** (1990) 425 [INSPIRE].

[57] Y. Ezawa et al., *Brown-Feynman reduction of one loop Feynman diagrams to scalar integrals with orthonormal basis tensors*, *Comput. Phys. Commun.* **69** (1992) 15 [INSPIRE].

[58] A.I. Davydychev, *A simple formula for reducing Feynman diagrams to scalar integrals*, *Phys. Lett.* **B 263** (1991) 107 [INSPIRE].

JHEP10(2011)070

[59] Z. Bern, L.J. Dixon and D.A. Kosower, *Dimensionally regulated one loop integrals*, *Phys. Lett.* **B 302** (1993) 299 [*Erratum ibid.* **B 318** (1993) 649] [hep-ph/9212308] [INSPIRE].

[60] Z. Bern, L.J. Dixon and D.A. Kosower, *Dimensionally regulated pentagon integrals*, *Nucl. Phys.* **B 412** (1994) 751 [hep-ph/9306240] [INSPIRE].

[61] O. Tarasov, *Connection between Feynman integrals having different values of the space-time dimension*, *Phys. Rev.* **D 54** (1996) 6479 [hep-th/9606018] [INSPIRE].

[62] J. Fleischer, F. Jegerlehner and O. Tarasov, *Algebraic reduction of one loop Feynman graph amplitudes*, *Nucl. Phys.* **B 566** (2000) 423 [hep-ph/9907327] [INSPIRE].

[63] T. Binoth, J. Guillet and G. Heinrich, *Reduction formalism for dimensionally regulated one loop N point integrals*, *Nucl. Phys.* **B 572** (2000) 361 [hep-ph/9911342] [INSPIRE].

[64] A. Denner and S. Dittmaier, *Reduction of one loop tensor five point integrals*, *Nucl. Phys.* **B 658** (2003) 175 [hep-ph/0212259] [INSPIRE].

[65] G. Duplancic and B. Nizic, *Reduction method for dimensionally regulated one loop N point Feynman integrals*, *Eur. Phys. J.* **C 35** (2004) 105 [hep-ph/0303184] [INSPIRE].

[66] W. Giele and E. Glover, *A calculational formalism for one loop integrals*, *JHEP* **04** (2004) 029 [hep-ph/0402152] [INSPIRE].

[67] W. Giele, E. Glover and G. Zanderighi, *Numerical evaluation of one-loop diagrams near exceptional momentum configurations*, *Nucl. Phys. Proc. Suppl.* **135** (2004) 275 [hep-ph/0407016] [INSPIRE].

[68] T. Binoth, J. Guillet, G. Heinrich, E. Pilon and C. Schubert, *An algebraic/numerical formalism for one-loop multi-leg amplitudes*, *JHEP* **10** (2005) 015 [hep-ph/0504267] [INSPIRE].

[69] R. Ellis, W. Giele and G. Zanderighi, *Semi-numerical evaluation of one-loop corrections*, *Phys. Rev.* **D 73** (2006) 014027 [hep-ph/0508308] [INSPIRE].

[70] A. Denner and S. Dittmaier, *Reduction schemes for one-loop tensor integrals*, *Nucl. Phys.* **B 734** (2006) 62 [hep-ph/0509141] [INSPIRE].

[71] R. Ellis, W. Giele and G. Zanderighi, *The one-loop amplitude for six-gluon scattering*, *JHEP* **05** (2006) 027 [hep-ph/0602185] [INSPIRE].

[72] T. Binoth, J. Guillet and G. Heinrich, *Algebraic evaluation of rational polynomials in one-loop amplitudes*, *JHEP* **02** (2007) 013 [hep-ph/0609054] [INSPIRE].

[73] T. Diakonidis et al., *On the tensor reduction of one-loop pentagons and hexagons*, *Nucl. Phys. Proc. Suppl.* **183** (2008) 109 [arXiv:0807.2984] [INSPIRE].

[74] T. Diakonidis et al., *A Complete reduction of one-loop tensor* 5 *and* 6*-point integrals*, *Phys. Rev.* **D 80** (2009) 036003 [arXiv:0812.2134] [INSPIRE].

[75] G. Ossola, C.G. Papadopoulos and R. Pittau, *Reduction of one-loop amplitudes at the integrand level: NLO QCD calculations*, *Acta Phys. Polon.* **B 39** (2008) 1685 [INSPIRE].

[76] W. Gong, Z. Nagy and D.E. Soper, *Direct numerical integration of one-loop Feynman diagrams for N-photon amplitudes*, *Phys. Rev.* **D 79** (2009) 033005 [arXiv:0812.3686] [INSPIRE].

[77] A. van Hameren, *Multi-gluon one-loop amplitudes using tensor integrals*, *JHEP* **07** (2009) 088 [arXiv:0905.1005] [INSPIRE].

JHEP10(2011)070

[78] G. Bélanger et al., *Automatic calculations in high energy physics and Grace at one-loop*, *Phys. Rept.* **430** (2006) 117 [hep-ph/0308080] [INSPIRE].

[79] F. del Aguila and R. Pittau, *Recursive numerical calculus of one-loop tensor integrals*, *JHEP* **07** (2004) 017 [hep-ph/0404120] [INSPIRE].

[80] A. van Hameren, J. Vollinga and S. Weinzierl, *Automated computation of one-loop integrals in massless theories*, *Eur. Phys. J.* **C 41** (2005) 361 [hep-ph/0502165] [INSPIRE].

[81] T. Binoth, J.-P. Guillet, G. Heinrich, E. Pilon and T. Reiter, *Golem95: a numerical program to calculate one-loop tensor integrals with up to six external legs*, *Comput. Phys. Commun.* **180** (2009) 2317 [arXiv:0810.0992] [INSPIRE].

[82] F. Campanario, C. Englert, M. Rauch and D. Zeppenfeld, *Precise predictions for $W\gamma\gamma$ + jet production at hadron colliders*, *Phys. Lett.* **B 704** (2011) 515 [arXiv:1106.4009] [INSPIRE].

[83] T. Reiter, *An automated approach for $q\bar{q}$ to$b\bar{b}b\bar{b}$ at Next-to-Leading Order QCD*, arXiv:0903.4648 [INSPIRE].

[84] Wolfram Research Inc., *Mathematica, version* 5.2, Champaign, U.S.A. (2005).

[85] R. Mertig, M. Böhm and A. Denner, *FEYN CALC: computer algebraic calculation of Feynman amplitudes*, *Comput. Phys. Commun.* **64** (1991) 345 [INSPIRE].

[86] K. Hagiwara and D. Zeppenfeld, *Helicity amplitudes for heavy lepton production in e^+e^- annihilation*, *Nucl. Phys.* **B 274** (1986) 1 [INSPIRE].

[87] K. Hagiwara and D. Zeppenfeld, *Amplitudes for multiparton processes involving a current at e^+e^-, $e^\pm p$ and hadron colliders*, *Nucl. Phys.* **B 313** (1989) 560 [INSPIRE].

[88] A. Bredenstein, A. Denner, S. Dittmaier and S. Pozzorini, *NLO QCD corrections to $t\bar{t}b\bar{b}$ production at the LHC: 1. Quark-antiquark annihilation*, *JHEP* **08** (2008) 108 [arXiv:0807.1248] [INSPIRE].

[89] F. Campanario, V. Hankele, C. Oleari, S. Prestel and D. Zeppenfeld, *QCD corrections to charged triple vector boson production with leptonic decay*, *Phys. Rev.* **D 78** (2008) 094012 [arXiv:0809.0790] [INSPIRE].

[90] G. Bozzi, F. Campanario, V. Hankele and D. Zeppenfeld, *NLO QCD corrections to $W^+W^-\gamma$ and $ZZ\gamma$ production with leptonic decays*, *Phys. Rev.* **D 81** (2010) 094030 [arXiv:0911.0438] [INSPIRE].

[91] G. Bozzi, F. Campanario, M. Rauch, H. Rzehak and D. Zeppenfeld, *NLO QCD corrections to $W^\pm Z\gamma$ production with leptonic decays*, *Phys. Lett.* **B 696** (2011) 380 [arXiv:1011.2206] [INSPIRE].

[92] G. Bozzi, F. Campanario, M. Rauch and D. Zeppenfeld, *$W^\pm\gamma\gamma$ production with leptonic decays at NLO QCD*, *Phys. Rev.* **D 83** (2011) 114035 [arXiv:1103.4613] [INSPIRE].

[93] F. Campanario, C. Englert and M. Spannowsky, *QCD corrections to non-standard WZ+jet production with leptonic decays at the LHC*, *Phys. Rev.* **D 82** (2010) 054015 [arXiv:1006.3090] [INSPIRE].

[94] A. Denner, S. Dittmaier, M. Roth and D. Wackeroth, *Predictions for all processes $e^+e^- \to 4$ fermions + γ*, *Nucl. Phys.* **B 560** (1999) 33 [hep-ph/9904472] [INSPIRE].

[95] S. Dittmaier, *Separation of soft and collinear singularities from one loop N point integrals*, *Nucl. Phys.* **B 675** (2003) 447 [hep-ph/0308246] [INSPIRE].

JHEP10(2011)070

[96] K. Arnold et al., *VBFNLO: A Parton level Monte Carlo for processes with electroweak bosons*, *Comput. Phys. Commun.* **180** (2009) 1661 [arXiv:0811.4559] [INSPIRE].

[97] K. Arnold, T. Figy, B. Jager and D. Zeppenfeld, *Next-to-leading order QCD corrections to Higgs boson production in association with a photon via weak-boson fusion at the LHC*, *JHEP* **08** (2010) 088 [arXiv:1006.4237] [INSPIRE].

[98] T. Figy, V. Hankele and D. Zeppenfeld, *Next-to-leading order QCD corrections to Higgs plus three jet production in vector-boson fusion*, *JHEP* **02** (2008) 076 [arXiv:0710.5621] [INSPIRE].

[99] H. Murayama, I. Watanabe and K. Hagiwara, *HELAS: HELicity Amplitude Subroutines for Feynman diagram evaluations*, KEK-91-11 (1991).

[100] J. Vermaseren, *Axodraw*, *Comput. Phys. Commun.* **83** (1994) 45 [INSPIRE].

JHEP10(2011)070